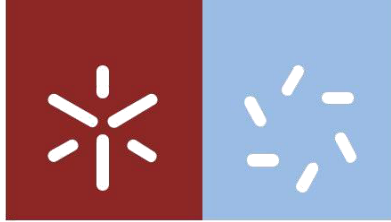


Universidade do Minho
Escola de Ciências

Tatiana Jorge Torres Vilhena Ventura

Development of nanostructured delivery scaffolds for doxorubicin via electrospinning



Universidade do Minho
Escola de Ciências

Tatiana Jorge Torres Vilhena Ventura

Development of nanostructured delivery scaffolds for
doxorubicin via electrospinning

Dissertação de Mestrado
Biofísica e Bionanossistemas

Trabalho efetuado sob a orientação da
Doutora Marlene Susana Dionísio Lúcio
e da
Doutora Teresa Maria Santos Ribeiro Viseu

DECLARAÇÃO

Nome: Tatiana Jorge Torres Vilhena Ventura

Endereço eletrónico: tatianaventura28@msn.com **Telefone:** 917490263

Número do Bilhete de Identidade: 14305674

Título dissertação: "Development of nanostructured delivery scaffolds for doxorubicin via electrospinning"

Orientador(es): Doutora Marlene Susana Dionísio Lúcio e Doutora Teresa Maria Santos Ribeiro Viseu

Ano de conclusão: 2018

Designação do Mestrado: Biofísica e Bionanossistemas

DE ACORDO COM A LEGISLAÇÃO EM VIGOR, NÃO É PERMITIDA A REPRODUÇÃO DE QUALQUER PARTE DESTA TESE/TRABALHO

Universidade do Minho, ___/___/_____

Assinatura: _____

Acknowledgments:

I would like to start by thanking all people and entities that made my dissertation possible.

First of all, I would like to thank my Professors, Professor Marlene Lúcio and Professor Teresa Viseu for all the trust, all the patience and all the commitment. For believing in me and for helping me when I needed, but most of all for the knowledge and for guiding me on this important moment of my academic formation. I thank you for all that you have done for me.

Professor Etelvina Gomes for receiving me in her laboratory and giving me free access to all the necessary equipment for the production of nanofibers via electrospinning. And I should be also thankful for all the availability and suggestions given for this dissertation.

Additionally, to PARALAB and SEMAT for the microscope images.

I would like to thank Doctor Raul Machado, Doctor Senentxu Lanceros-Méndez and Doctor Clarisse Ribeiro for all the analysis that contributed for the development of this dissertation.

And Professor Ana Preto and Ana Rita Brás for their availability and for the cellular assays in the colorectal cancer cell lines.

Now I would like to thank my laboratory colleagues, Tiago Costa and Pedro Rêgo, for assisting me through this long path and always being there for me and for all the good moments we share in the laboratory and in the university.

My friend Maria, for supporting and believing in me even though she was not present all the time. And Fábio for being the person that believed in me the most, for cheering me up when things were not so bright and for giving me the support I needed

I would like to thank my athletes for being so patient in this last year and for all the encourage words.

And last but not least, my family, especially my parents, the ones that believe in me the most and always pushed me to do my best, and I'm sure that without their support none of this would be possible. Thank You very much.

Abstract

Doxorubicin (DOX) is a class I (high permeability and high solubility) anthracycline antibiotic widely used as a chemotherapeutic drug for treating many types of cancers. It can induce apoptosis of cancerous cells by damaging DNA and its replication via the mechanisms of intercalation between nucleotides, by inhibition of topoisomerase-II and by generating oxygen free radicals. However, free DOX is known to have a very low therapeutic index and repeated administration of high doses are required to achieve the desirable therapeutic effect, which causes severe side effects to normal tissues like cardiotoxicity and myelosuppression. So, the development of suitable carrier systems for local treatment of cancer recurrence is necessary. Recent studies indicate that an enhanced therapeutic efficacy can be achieved by using nanocarriers that accomplish rapid drug release once they arrive at the tumor site. It is recognized that the use of electrospun nanofibers for drug carriers is very promising in the biomedical field, mainly for the local chemotherapy postoperation.

The objective of this study is to develop a novel system for local application of DOX either in surgical locci or in a topical application device enabling a controlled release of the drug. The developed system involves the encapsulation of DOX into electrospun polymeric nanofibers. Chosen polymers were poly (ethylene oxide) (PEO) and poly (ϵ -caprolactone) (PCL), because they are both biocompatible and biodegradable, and are approved by FDA, and chitosan (CS) which is a biocompatible natural polymer.

Nanofibers' composition and preparation methods were optimized for the two polymeric systems. Topographic and morphologic characterization were done by Scanning Electron Microscopy (SEM). Crystalline structural characterization of the produced nanofibers was achieved by differential scanning calorimetry (DSC) and X-ray diffraction evidencing the presence of DOX inside the fibers. To elucidate the interactions between the polymer and DOX, as well as, to analyze the chemical composition, Attenuated Total Reflectance Fourier Transform Infrared Spectroscopy (ATR-FTIR) and Nuclear Magnetic Resonance (NMR) were used. To know more about the surface properties of the nanofibers produced, contact angles of water on the surface of the electrospun nanofibers were measured. Mechanical properties of the nanofibers were also evaluated by stress-strain tests. Controlled release assays were carried out at cancer tissues' conditions (pH 5.5 and 37°C). The kinetics of DOX release from PEO-loaded with and without CS, and from PCL-loaded nanofibers was established and can be tailored adjusting electrospinning conditions and drug load capacity. The sulforhodamine B (SRB) assay was also performed to measure drug-induced cytotoxicity in human colorectal cancer cell line HCT-116.

Resumo

A doxorubicina (DOX) é uma antraciclina pertencente à classe I (elevada permeabilidade e elevada solubilidade) muito usada como fármaco anticancerígeno. A DOX pode induzir a apoptose das células cancerígenas danificando o ADN e interferindo na sua replicação através de mecanismos de intercalação entre os nucleótidos, por inibição da topoisomerase-II e por gerar radicais livres de oxigénio. Contudo, a DOX é conhecida por ter um baixo índice terapêutico sendo necessárias elevadas doses e administrações repetidas para obter o efeito terapêutico desejado, causando efeitos secundários severos tais como cardiotoxicidade e mielossupressão. Estudos recentes indicam que se pode alcançar uma melhor eficácia de tratamento usando nano transportadores para a entrega local de fármacos para quimioterapia local após cirurgias.

O objetivo deste trabalho é desenvolver um sistema contendo DOX para aplicação local tanto na loca cirúrgica após extração do tumor, como na forma de um dispositivo de aplicação tópica que permita a libertação controlada do fármaco onde for necessário. O sistema desenvolvido envolve a encapsulação da DOX em nanofibras poliméricas produzidas por *electrospinning*. Os polímeros escolhidos foram o óxido de polietileno (PEO) e a policaprolatona (PCL) devido à sua biocompatibilidade e biodegradabilidade e por serem aprovados pela FDA, e o quitosano (CS) por ser um polímero natural biocompatível.

A composição e o método de preparação das nanofibras foram otimizados para os dois sistemas poliméricos. A caracterização topográfica e morfológica foi realizada por Microscopia Electrónica de Varrimento (SEM). A caracterização estrutural cristalina das nanofibras produzidas foi efetuada por calorimetria diferencial de varrimento (DSC) e por difração de Raios-X que evidenciaram ainda a presença de DOX dentro das fibras. As propriedades mecânicas foram avaliadas por testes de tensão e *stress*. Para elucidar acerca das interações entre os polímeros e a DOX, assim como para analisar a composição química das fibras, foi usada a Espectroscopia de Absorção no Infravermelho por Transformada de Fourier (ATR-FTIR) e a Ressonância Magnética Nuclear (NMR). Para saber mais sobre as propriedades da superfície das nanofibras, foram medidos os ângulos de contacto com a água. Os ensaios de libertação controlada do fármaco foram realizados sob condições miméticas dos tecidos cancerígenos (pH 5.5 e a 37°C). A cinética da libertação de DOX das nanofibras de PEO com e sem CS e das nanofibras de PCL foi avaliada e poderá ser alterada ajustando as condições do *electrospinning* e a capacidade de encapsulamento do fármaco. O ensaio de sulforodamina B (SRB) foi também realizado para medir a citotoxicidade induzida pelo fármaco na linha celular do cancro colorectal HCT-116.

TABLE OF CONTENTS

ACKNOWLEDGMENTS.....	III
ABSTRACT.....	V
RESUMO.....	VII
ABBREVIATIONS.....	XI
FIGURES INDEX.....	XIII
TABLES INDEX.....	XIV
1 INTRODUCTION	15
1.1 CANCER: INCIDENCE AND IMPACT	15
1.2 COLORECTAL CANCER: THERAPEUTIC CHALLENGES	15
1.3 DOXORUBICIN IN CANCER THERAPY.....	17
1.4 ELECTROSPUN POLYMERIC NANOFIBERS AS DRUG DELIVERY SYSTEMS FOR CANCER THERAPY	21
1.5 WORKING HYPOTHESIS AND OBJECTIVES OF THIS WORK	24
2 EXPERIMENTAL SECTION	25
2.1 MATERIALS	25
2.2 PREPARATION OF POLYMERIC SOLUTIONS	26
2.3 PRODUCTION OF THE NANOFIBERS BY ELECTROSPINNING.....	27
2.4 CHARACTERIZATION OF THE POLYMERIC NANOFIBERS.....	28
2.4.1 Topographic and morphologic characterization	28
2.4.2 Crystalline structure and thermic behavior	29
2.4.3 Mechanical properties	29
2.4.4 Chemical composition	30
2.4.5 Surface properties characterization	31
2.5 EVALUATION OF THE POLYMERIC NANOFIBERS THERAPEUTIC PERFORMANCE	31
2.5.1 Control release assays under biological mimetic conditions	31
2.5.2 Cytotoxicity studies in a relevant cancer cell line	32
3 RESULTS AND DISCUSSION.....	33
3.1 TOPOGRAPHIC AND MORPHOLOGIC CHARACTERIZATION OF PEO AND PCL NANOFIBERS	33
3.2 CRYSTALLINE STRUCTURE AND THERMIC BEHAVIOR OF PEO AND PCL NANOFIBERS	35
3.3 MECHANICAL PROPERTIES OF PEO AND PCL NANOFIBERS	36
3.4 CHEMICAL COMPOSITION OF PEO AND PCL NANOFIBERS	37
3.5 SURFACE PROPERTIES CHARACTERIZATION OF PEO AND PCL NANOFIBERS	40
3.6 EVALUATION OF THE PEO AND PCL NANOFIBERS THERAPEUTIC PERFORMANCE.....	41
3.6.1 Control release assays of DOX loaded PEO nanofibers under biological mimetic conditions	41
3.6.2 Stability studies of DOX in presence of PEO or PEO-CS	45
3.6.3 Control release assays of DOX loaded PCL nanofibers under biological mimetic conditions	51
3.6.4 Cytotoxicity studies of DOX loaded PEO or PCL nanofibers in colorectal cancer cell lines	56
4 CONCLUSIONS AND FUTURE PERSPECTIVES.....	58
5 BIBLIOGRAPHY	60

Abbreviations

ATR-FTIR	Attenuated total reflectance Fourier transform infrared spectroscopy
CRC	Colorectal cancer
CS	Chitosan
DMEM	Dulbecco's Modified Eagle Medium
DNA	Deoxyribonucleic Acid
DSC	Differential scanning calorimetry
DOX	Doxorubicin
FDA	Food and drug administration
HCT	Human colon tumor cells
NHMAAm	N-hydroxymethylacrylamide
NIPAAm	N-isopropylacrylamide
NMR	Nuclear magnetic resonance
PBS	Phosphate buffered saline
PCL	Poly(ϵ -caprolactone)
PCL-PEG-PCL	Poly(ϵ -caprolactone)-poly(ethyleneglycol)-poly(ϵ caprolactone)
PEG-PLLA	Polyethylene glycol-Poly(L-lactic acid)
PEO-CS-GO	Polyethylene oxide-chitosan with graphene oxide dots
PLGA-CNT	Poly(lactic acid-co-glycolic acid) with carbon nanotubes
PLGA-n-HA	Poly(lactic acid-co-glycolic acid) with hydroxyapatite nanoparticles
PLLA	Poly(L-lactic acid)
PLLA-MSN	Poly(L-lactic acid) with mesoporous silica nanoparticles
(P(NIPAAm-NHMAAm)-MNP	Poly(N-isopropylacrylamide-co-N-hydroxymethylacrylamide) with magnetic nanoparticles
P(NIPAAm-AAm-VP)	Poly(N-isopropylacrylamide-co-acrylamide-co-vinylpyrrolidone)
PVA-CS	Polyvinyl alcohol-chitosan
SEM	Scanning electron microscopy
SLS	Sodium lauryl sulphate
SRB	Sulforhodamine B
XRD	X-ray diffraction

Figures Index

Figure 1 - Estimated number of incident cases and deaths in both sexes, Portugal (top 10 cancer types) in 2012. Graph produced in Global Cancer Observatory (http://gco.iarc.fr/).....	16
Figure 2 - Doxorubicin chemical structure. Tetracyclic ring (anthracyclinone) bonded to daunosamine sugar.....	18
Figure 3 - Mechanisms of therapeutic action of doxorubicin (DOX).....	20
Figure 4 - PEO: Poly(ethylene oxide); PCL: Poly(ϵ -caprolactone) and CS: Chitosan.....	23
Figure 5 – (A) Photographic image of homemade electrospinning setup.....	27
Figure 6 – SEM image of PEO nanofibers (4100x) and histogram of the diameters distribution of these fibers.....	33
Figure 7 – SEM image of PCL nanofibers (4100x) and histogram of the diameters distribution of these fibers.....	34
Figure 8 – SEM image of a PCL mat, cut in liquid nitrogen, showing the thickness of the mat.....	34
Figure 9 - XRD spectra of polymer nanofibers (PEO and PCL) without and with DOX encapsulation (blue lines are peaks assigned to the polymer while red lines are possible DOX peaks).....	35
Figure 10 - DSC curves for PCL and PEO nanofibers without and with DOX incorporation.....	36
Figure 11 – Stress-strain curve for PCL and PEO fibers without and with DOX incorporation.....	37
Figure 12 – ATR-FTIR spectra of PEO and PEO-DOX (1.75 wt%) nanofibers. Also shown, for comparison, ATR-FTIR spectra of DOX (powder).....	38
Figure 13 – ATR-FTIR spectra of PCL and PCL-DOX (8.33 wt%) nanofibers. Also shown, for comparison, ATR-FTIR spectra of DOX (powder). Red lines identify bands attributed to DOX.....	39
Figure 14 – Schematic view of superhydrophilic, hydrophilic, hydrophobic, and superhydrophobic surfaces classifications according to the water contact angle. Adapted from [73].....	40
Figure 15 – Water contact angles and corresponding shapes of water droplets for electrospun PEO and PCL nanofibrous mats in the absence and in presence of different DOX contents.....	41
Figure 16 – Control release of PEO-DOX (1.75 wt%) nanofibers in buffer pH \approx 5.5 (three replicas). Dashed lines are only eye guides.....	42
Figure 17 – Control release of PEO–CS- DOX (1.75 wt%) nanofibers in buffer pH \approx 5.5 using three different CS content. Dashed lines are only eye guides.....	43
Figure 18 – Control release of PEO-DOX (1.75 wt%) nanofibers placed into a dialysis bag in buffer pH \approx 5.5. Also shown a photograph of the dialysis bag at the end of the assay. Dashed lines are only eye guides. The cartoon elucidates the procedure of control release assay in a dialysis bag.....	44
Figure 19 – Absorbance versus time for DOX and PEO-DOX in buffer solutions (pH \approx 5.5). Inset (I) shows in more detail the absorbance decrease of DOX in PEO-DOX buffered solutions for the first 9 hours.....	45
Figure 20 – Control release of PEO-DOX (1.75 wt%) nanofibers in buffer pH \approx 5.5 and in acetic acid. Dashed lines are only eye guides.....	46
Figure 21 – Solutions of PEO+DOX powders in buffer pH \approx 5.5 and in strong acid (acetic acid 90%) and representation of possible PEO-DOX interaction trough hydrogen bonding.....	47
Figure 22 – NMR spectra of PEO-DOX and PEO-CS-DOX obtained from drying control release medium and posterior dissolution of residues in deuterated water.....	48
Figure 23 – NMR spectra of PEO-DOX and PEO-CS-DOX obtained from drying control release medium and posterior dissolution of residues in deuterated water (detail of the 2-3 ppm region). Red dashed lines assign the location of NMR bands in PEO-DOX residues. These bands are shifted of about 0.5 ppm in PEO-CS-DOX residues (blue arrows indicate the shift).....	49
Figure 24 – NMR spectra of DOX (powder) and PEO (powder) in deuterated water.....	49
Figure 25 – ATR-FTIR spectra from the dried residual gels that remained inside the dialysis bag at the end of the control release assay of PEO-DOX and PEO-CS-DOX nanofibers. For comparison DOX (powder) and PEO (nude nanofibers) spectra are also shown.....	50
Figure 26 – Control release of PCL-DOX nanofibers in buffer pH \approx 5.5 using four different DOX content. Dashed lines are only eye guides.....	51
Figure 27 – Control release of PCL-DOX nanofibers in buffer pH \approx 5.5 using four different DOX contents evidencing the great variability between replicas. Dashed lines are only eye guides.....	52
Figure 28 – Control release of PCL-DOX (1.75 wt%) nanofibers in buffer pH \approx 5.5. After 2 hours (at the blue arrow point) the fibers were carefully withdrawn from the buffer solution and were put into a fresh release medium. Dashed lines are only eye guides.....	53
Figure 29 – Control release of PCL-DOX nanofibers in micellar medium (SLS 16 mM, pH 5.5) using three different DOX content. Dashed lines are only eye guides.....	54

Figure 30 – Control release of PCL-DOX nanofibers, confined into a dialysis bag, in buffer pH \approx 5.5, using four different DOX content. Two replicas are depicted for each drug concentration. Dashed lines are only eye guides.	55
Figure 31 – Control release of PCL-DOX (1.39 wt%) nanofibers, confined into a dialysis bag, in buffer pH \approx 5.5. Six replicas are depicted. Dashed lines are only eye guides.....	56
Figure 32 – Cytotoxicity of free DOX and DOX encapsulated into PEO and PCL nanofibers, against HCT-116 colorectal tumour cells.	57

Tables Index

Table 1 – Used reagents and solvents.....	25
Table 2 – Polymeric solutions used in the production of eletrospun nanofibers	26

1 INTRODUCTION

1.1 CANCER: INCIDENCE AND IMPACT

Cancer, also known as malignant tumor or neoplasm, is a generic designation for a vast group of pathologies that can affect distinct organs or tissues of the human body. One common feature of cancer is the rapid division and propagation of abnormal cells that grow beyond their usual boundaries, and which can then invade neighboring tissues and spread and reach other parts of the body through blood vessels and lymphatic systems, a process referred as metastasizing. Metastases are a major cause of death from cancer [1, 2].

In spite of many therapeutic developments, cancer remains a leading cause of death worldwide, with a mortality of 8.8 million people in 2015. The World Health Organization (WHO) and International Agency for Research on Cancer (IARC) reveal that, the incidence of all cancer cases will rise to 21.2 million by 2030. The economic impact of cancer is significant and is increasing. The total annual economic cost of cancer in 2010 was estimated at approximately US\$ 1.16 trillion [3, 4]. In the European Union, cancer has also a growing severe economic and social impact since that it is also the second most common cause of death [3, 5, 6]. Similarly to what happens in other European countries, in Portugal, 24.3% of all mortality cases are due to cancer, which makes this disease the second cause of death only surpassed by circulatory and cardiac diseases [7].

1.2 COLORECTAL CANCER: THERAPEUTIC CHALLENGES

Currently, the most common causes of cancer world death are cancers of lung (1.69 million deaths), liver (788 000 deaths), colorectal (774 000 deaths), stomach (754 000 deaths) and breast (571 000 deaths) [3, 8]. From these types of cancers, the colorectal cancer (CRC) is one of the most aggressive malign cancers [9]. In Portugal CRC is the first most common cancer, showing an incidence and mortality rate of 14% and 16% respectively (Figure 1) [3, 10]

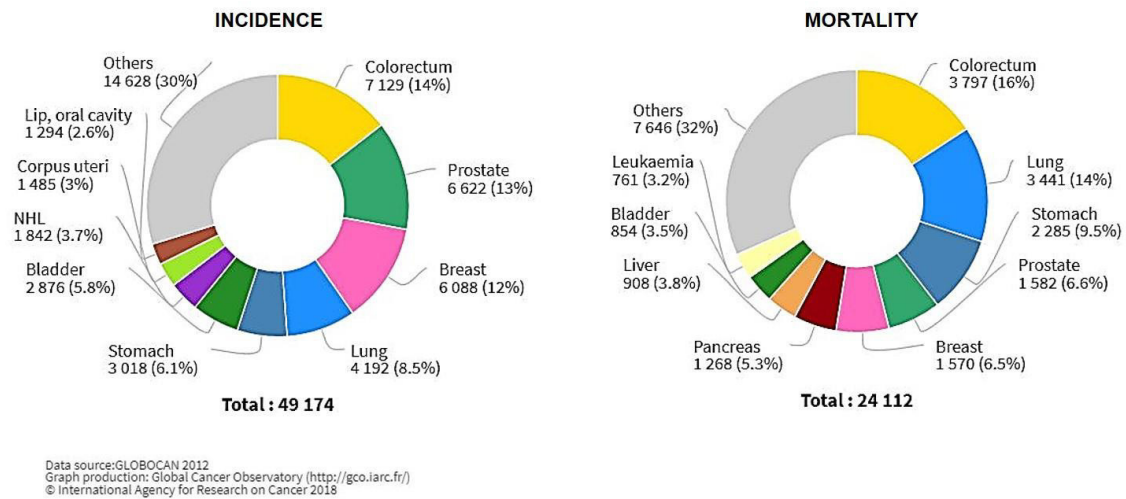


Figure 1 - Estimated number of incident cases and deaths in both sexes, Portugal (top 10 cancer types) in 2012. Graph produced in Global Cancer Observatory (<http://gco.iarc.fr/>).

CRC is a result of several unmodifiable risks factors, such as aging, personal history of adenomatous polyps and inflammatory bowel disease, family history of CRC and inherited genetic risk of CRC. In addition, a substantial number of environmental and lifestyle risk factors may play an important role in the development of CRC such as bad nutritional practices, low physical activity and obesity, smoking and heavy alcohol consumption [9].

CRC usually begins with adenomatous polyps in the intestine, which can be defined as well demarcated masses of epithelial dysplasia, with uncontrolled crypt cell division. These adenomatous polyps are considered malignant when anomalous cell proliferation invades progressively other intestinal tissue layers nearby and spread to distant organs. At this point CRC creates metastases and reaches other organs through lymphatic systems (in 30-50% of the patients) and blood vessels (in 10-30% of the cases) [11].

One of the therapeutic challenges of CRC is that the symptoms and signs are noticeable only at late stages of the disease development when the prognosis is poor, being difficult to detect the cancer and treat it at an early phase. Common symptoms and signs include abdominal pain, change in bowel habits, blood in feces, weakness or malaise, involuntary weight loss and anemia [12]. Nowadays, surgery and chemotherapy are the two main therapeutic options for CRC, depending on the cancer stages and tumor location at diagnosis, as well as individual characteristics of the patients. Surgery is the most common treatment to remove the cancer in an early stage (stage I and II). For patients in stage III and some patients in stage II, surgery is followed by approximately 6 months of chemotherapy. Patients with stage II and III rectal cancers are often

treated with neoadjuvant chemotherapy combined with radiation. Chemotherapy is often the main treatment of patients with advanced CRC (stage IV). A growing number of target drugs are also available to treat metastasizing CRC [8, 13, 14].

Another important challenge faced by CRC therapy is the disease recurrence that, depending on the location and aggressiveness of the disease, is developed by the patients that have been treated with surgery [15, 16]. Indeed, about 20-30% stage II and 50-60% stage III patients will relapse within 5 years after radical surgery with poor prognosis [15, 16]. To minimize the risk of recurrence, chemotherapy would be the most curative treatment option for CRC after surgery being performed. However, anticancer drugs are usually systemically administered and its circulation within the blood exposes, not just tumor cells but all other body organs, to the toxicity of the drugs. Hence, the risk of systemic toxicity outweighs the potential benefit of performing chemotherapy after surgery to avoid recurrence in CRC patients [15].

Drug resistance is the third most important challenge that opposes to successful therapy of CRC. It develops in almost all CRC patients, and limits the therapeutic efficacies of anticancer agents leading to chemotherapy failure, even though the response rate to current systemic chemotherapies can reach up to 50% [14, 17]. Among other causes, it has been recently proposed that drug resistance may arise from the high circulatory doses of anticancer drugs, which besides being aggressive and toxic to the healthy tissues, is more likely to result in the return of the cancer. This recent approach to cancer therapy suggests that classical systemic high-dosage treatments allow drug-resistant cancer cells to still survive. Then, with no other cancer cells to compete with, the drug-resistant cancer cells can quickly replicate and return as a far more aggressive form of cancer [18].

In conclusion, as the classic therapeutic strategies used in the CRC treatment show many challenges it is essential to develop new therapeutic approaches to minimize those and provide a better life for patients. Currently, investment of research should be in new therapies and technologies that are less invasive, less toxic and with a local application, which leads to a decrease of the side effects and better results.

1.3 DOXORUBICIN IN CANCER THERAPY

Doxorubicin (DOX) is a nonselective class I anthracycline, a group of anticancer antibiotics first obtained from *Streptomyces peucetius* [19]. DOX has shown great treatment potential, being regarded as one of the most potent of the Food and Drug Administration (FDA) approved

chemotherapeutic drugs [20]. It is widely used in solid tumors treatment in clinical practice and in chemotherapy, due to its efficiency in fighting a wide range of cancers such as carcinomas, sarcomas and hematological neoplasias [21] and has also efficacy in CRC although presenting some limitations that include drug resistance and high toxicity [21-25]. Despite the therapeutic potency of DOX, its pharmacokinetics reveals several drawbacks. DOX half-life is about 3-5 minutes, and by not being specifically targeted to tumors, it could change the growth of the other cells types in the body. Indeed, DOX shows a very fast distribution on vital organs, such as heart, lungs, liver and kidneys. Contrastingly, DOX takes longer times to be eliminated from the tissues increasing the toxicity risk in the healthy organs. This problem frequently results in severe toxicity and immunologic system fragility, which can lead to microbial infections, fatigue and decrease of healing time. Given the short half-life of DOX and its wide distribution across body tissues, this drug has to be administrated frequently and in high doses to allow enough dose to reach tumor tissues. However these therapeutic regimes (high doses, high frequency of administration) further increase the drug toxicity [19, 20, 26].

Chemically, DOX is composed by a quinone and a hydroquinone tetracyclic ring (anthracyclinone) bonded to a daunosamine sugar (Figure 2).

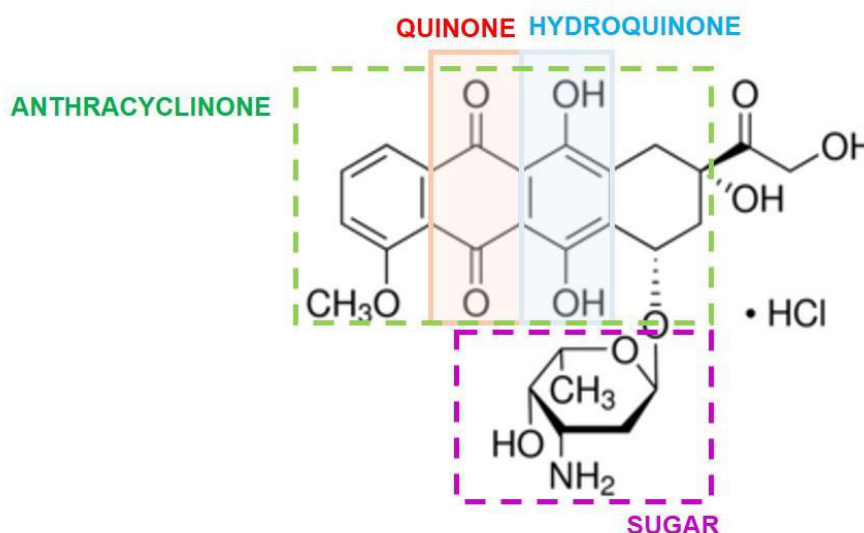
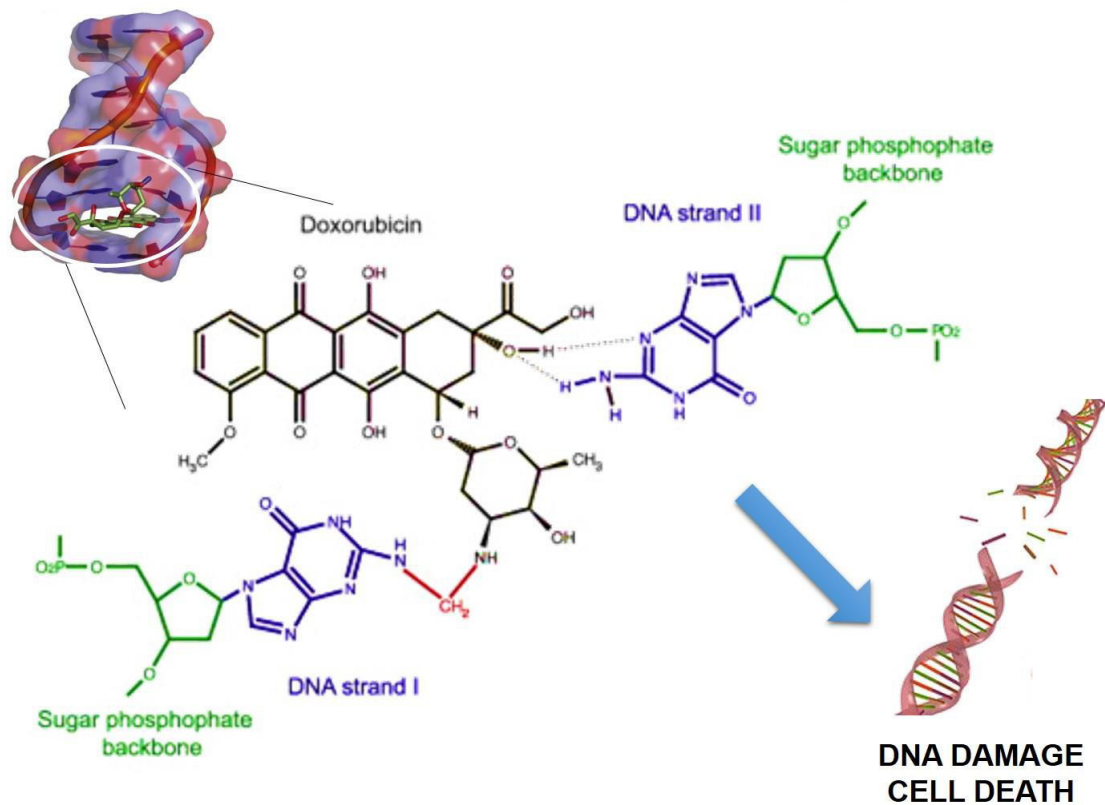


Figure 2 - Doxorubicin chemical structure. Tetracyclic ring (anthracyclinone) bonded to daunosamine sugar.

The presence of quinone and hydroquinone moieties on adjacent rings enhance the loss of electrons and consequently the propensity of DOX being oxidized to semiquinone, an unstable metabolite, which quickly reacts with oxygen to generate reactive oxygen species such as

superoxide and hydrogen peroxide radicals (Figure 3). These reactive oxygen species can then lead to lipid peroxidation and membrane damage, DNA damage, oxidative stress, and trigger apoptotic pathways of cell death being a possible mechanism responsible for the anticancer effect of this drug [19, 27]. Another proposed mechanism by which DOX acts in cancer cells is by binding to DNA and intercalating between the DNA bases. As a consequence, intercalation involves an increase in the vertical separation between adjacent base pairs and partial unwinding of the double helix, causing changes of the twist angle and distortions of the sugar-phosphate backbone. This leads to the inhibition of both DNA and RNA polymerase, ultimately ceasing DNA replication and RNA transcription (Figure 3). Furthermore, the cellular attempt to revert the DOX induced DNA breaks fail because this drug is also responsible by the inhibition of topoisomerase-II, an enzyme involved in DNA repair. By binding to all these molecular targets, DOX triggers the apoptosis pathway and inhibits cellular growth [20]. X-ray crystallography studies and molecular simulations have proved that these later mechanisms of action are also dependent on DOX special chemistry and molecular structure. To be able to intercalate in the cellular DNA, DOX planar chromophores insert between DNA bases and anchor to them by establishing covalent and hydrogen bonding [28-30]. Therefore, the presence of a planar aromatic or heteroaromatic ring system of appropriate dimensions and geometry that fits between adjacent base pairs of DNA is an essential requirement for DNA intercalation and consequently for DOX therapeutic outcome [28-30]. In case of DOX tetracyclic ring suffers chemical degradation or in case of administration of high DOX concentrations, where a molecular dimerization occurs, DOX may lose its therapeutic efficiency as based on simple geometric considerations, it is obvious that in these situations the DNA intercalation is hindered [31, 32].

1. INTERCALATION INTO DNA AND INHIBITION OF TOPOISOMERASE



2. PRODUCTION OF REACTIVE OXYGEN SPECIES

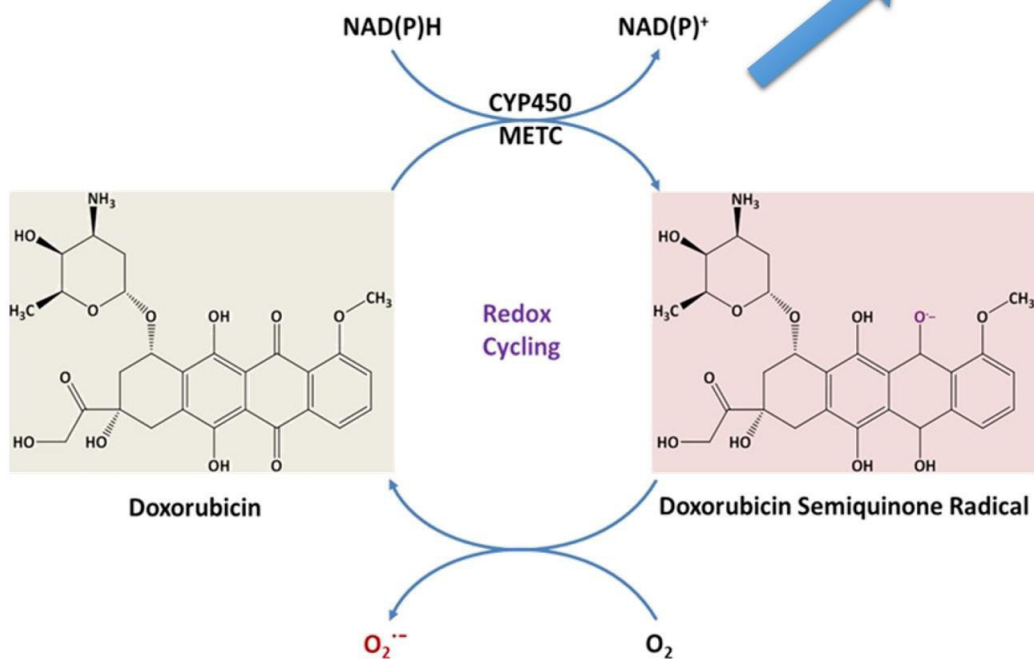


Figure 3 - Mechanisms of therapeutic action of doxorubicin (DOX).

Adapted from [27, 28]

1.4 ELECTROSPUN POLYMERIC NANOFIBERS AS DRUG DELIVERY SYSTEMS FOR CANCER THERAPY

Chemotherapy is the primary treatment practice responsible for treating millions of cancer patients. However, these treatments face important challenges like the anticancer drugs used that are not selective for killing tumor cells and eliminate normal healthy cells as well, especially those that divide faster. This leads to tissue toxicity and ultimately to organ toxicity because multiple cells are destroyed. Some cells responsible for triggering body's crucial immune responses are affected, which culminates in depression of the patients' immune system increasing their risk of developing viral or bacterial infections [20]. Therefore, it is necessary to produce new drug delivery systems able to carry drugs into the body and provide the delivery of appropriate therapeutic doses at the target site, increasing the efficiency and safety, through a controlled way, location and time of drug release [33].

There are two main targeted drug delivery methods. The first is a nanoparticle-based method, where various nanocarriers including polymeric micelles, nanoparticles (lipidic, polymeric or inorganic) and liposomes are designed to encapsulate drugs while their surface is chemically functionalized with targeting moieties meant to be recognized by specific cell receptors from the target tissues. These nanocarriers will be administrated far from the target tissues, but their targeting strategies will be responsible for delivering the drug they carry to a specific site, thus reducing the probability of affecting unwanted tissues [34, 35]. The second method is local administration of a drug delivery system. The drug-loading system is implanted at the aimed tumor site for the sake of locally delivering a dose of the drug and effectively eliminating the harm by migration from the bloodstream into the target tissue [36]. Locally controlled release systems that can be implanted and do not require surgical removal become a new tendency and have numerous advantages compared to conventional dosage forms, such as improved therapeutic effect, reduced toxicity, reduced frequency of drug administrations, and convenience [36, 37]. These local controlled release systems are a particularly good therapeutic choice for the prevention of post-surgery tumor recurrence, rather than systemic chemotherapy [38]. Therefore implantable local drug delivery systems that integrate anticancer drugs into a biodegradable scaffold can be a desirable solution for tumor recurrence that remains a major clinical problem following surgical treatment for most cancers such as lung, breast, head and neck, colorectal and prostatic cancers [39]. Many types of implantable local drug delivery systems have been reported, including gels, rods, wafers, films, and fibers all of which deliver a dose of drug directly to the target site. Often,

the mechanism of release from these scaffolds is diffusion or degradation depending on the polymeric system where the drug is embedded [40].

Between the mentioned implantable nanocarrier systems, nanofibers have recently received significant attentions for their advantages in biomedical applications. The manufacture of the nanofibers is accomplished by several methods such as template, self-assembly, phase separation, melt-blown, and electrospinning [41]. Electrospinning is a simple, cheap and very versatile technique and the only of these methods that can be scaled up for the mass production of continuous nanofibers from polymers, composites, semiconductors, and ceramics [41]. For this reason, electrospinning has gained significant interest in the last years not only in scientific community but also in industry. The versatility of electrospinning comes also from the fact that when conveniently adjusted all the parameters that affect the process, it allows making fibers of a huge variety of polymers, naturals and synthetics, with a great variety of diameters and morphologies [42-45].

Electrospun nanofibers are known as excellent drug carriers by providing large surface area-to-volume ratio for high drug loading and encapsulation efficiency, and a three-dimensional open porous structure, which provides an increase in the total fraction of drug that can be released. In addition, the inherent merits of electrospun nanofibers, such as the flexible handling, adjustable morphology, and good mechanical strength, offer many opportunities for them to be used as therapeutic implantable scaffolds be intratumorally, or adjacent to tumor, or at the surgical resection margins for cancer chemotherapy of solid tumors. Another advantage is that the electrospinning process affords great flexibility in producing polymeric fibers with customizable fiber size, porosity, drug loading rate and release mechanisms, leading to a possibility of tailoring the drug release rate for each application [37, 41, 42, 44, 46-49].

Various polymers have been electrospun into fibers and used to encapsulate DOX aiming an application for postoperative local chemotherapy. For example poly (ϵ -caprolactone)-poly (ethylene glycol)-poly(ϵ -caprolactone)(PCL-PEG-PCL) [41]; Polyethylene oxide-chitosan with graphene oxide dots (PEO-CS-GO)[45]; Poly(L-lactic acid) (PLLA)[38, 50]; Poly(L-lactic acid) with mesoporous silica nanoparticles (PLLA-MSN)[39, 48]; Polyethylene glycol-Poly(L-lactic acid) (PEG-PLLA) [37, 43, 51, 52]; Poly(lactic acid-co-glycolic acid) with carbon nanotubes (PLGA-CNT) [49]; Poly(lactic acid-co-glycolic acid) with hydroxyapatite nanoparticles (PLGA-n-HA)[46]; Polyvinyl alcohol-chitosan (PVA-CS) [53] and stimuli sensitive polymers like copolymer of N-isopropylacrylamide (NIPAAm) and

N-hydroxymethylacrylamide (NHMAAm) with magnetic nanoparticles, (P(NIPAAm-NHMAAm)-MNP) [54] and Poly(N-isopropylacrylamide-co-acrylamide-co-vinylpyrrolidone) (P(NIPAAM-AAm-VP) [55].

In the current work, polymers of contrasting chemical properties were used for the production of electrospun nanofibers loaded with DOX. Poly(ethylene oxide) (PEO), is a synthetic polyether (Figure 4) that is readily available in a range of molecular weights. These polymers are hydrophilic and soluble in water. PEO has been found to be biocompatible as it is nontoxic and approved by the FDA for use as excipients or as a carrier in different pharmaceutical formulations, foods, and cosmetics [56]. Most PEO are biodegradable or rapidly removed from the body unaltered with clearance rates inversely proportional to polymer molecular weight [57]. This property, combined with the availability of PEO with a wide range of end-functions, contributes to the wide use of PEO in biomedical research: drug delivery, tissue engineering scaffolds, surface functionalization, and many other applications [58]. PEO was combined with natural polymer, chitosan (CS) (Figure 4). CS due to the unique characteristics such as excellent biocompatibility, biodegradability, and nontoxicity has been widely used for drug delivery systems. However, the electrospinning of neat CS due to the low solubility, low stability and low mechanical properties is extremely difficult and thus it is normally blended with other polymers [45]. Poly(ϵ -caprolactone) (PCL) (Figure 4) is a semi crystalline hydrophobic, biodegradable polyester approved by FDA and widely used in biomedical applications as a drug delivery agent because of its cost efficiency, high mechanical resistance and biocompatibility. PCL possesses some unique properties such as the fact of degrading slower than other biodegradable polyesters in physiological condition, and this property can be exploited in the controlled release of drugs in target tissues over a period of time [59].

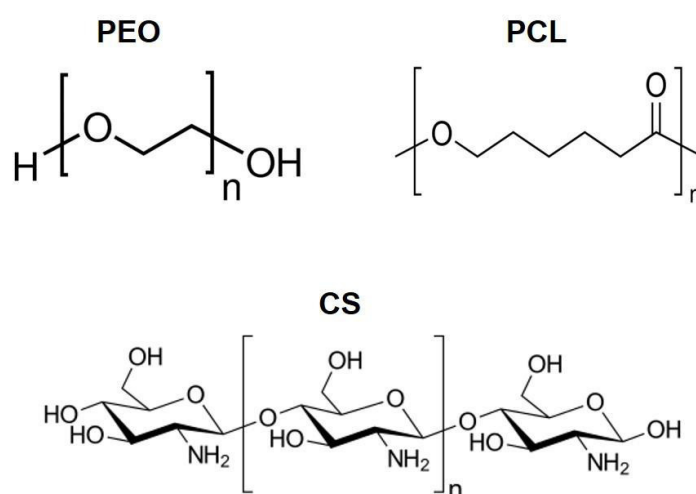


Figure 4 - PEO: Poly(ethylene oxide); PCL: Poly(ϵ -caprolactone) and CS: Chitosan

1.5 WORKING HYPOTHESIS AND OBJECTIVES OF THIS WORK

The first nanocarrier system approved by FDA for DOX delivery was a liposomal system launched in 1995 as Doxil® [60]. Since then thousands of different reports have addressed the design of nanocarrier systems in an attempt of enhancing DOX therapeutic performance, however important challenges still persist regarding its delivery to target tissues and few attempts have been made for a local direct administration of this drug.

Also, with the advent of interesting new polymeric scaffolds, new opportunities are opened to optimize the delivery of anticancer drugs like DOX. In this regard, the main objective of the present study is the production of electrospun nanostructured scaffolds loaded with doxorubicin to delivery this drug locally in surgical locci in colorectal cancer. These scaffolds consisted in polymeric nanofibers produced with two biocompatible and biodegradable polymers, with contrasting chemical properties: poly(ϵ -caprolactone) (PCL), a highly hydrophobic polymer and polyethylene oxide (PEO), a highly hydrophylic one.

As working hypothesis several questions were addressed during this work:

- (i) Are PEO or PCL nanofibers able to encapsulate DOX?
- (ii) Have PEO or PCL nanofibers adequate mechanic properties?
- (iii) What are the effects on the polymeric nanofibers when the drug is encapsulated?
- (iv) Are PEO or PCL nanofibers able to release DOX in a controlled way?
- (v) Are PEO or PCL nanofibers effective as citotoxic delivery systems for colorectal cancer cells?

To answer the above questions, specific goals were pursued such as a thorough characterization of the nanofibers mats produced, regarding its topologic surface, morfology, diameter, porosity, chemical composition, cristalinity and mechanical properties. After that the polymeric nanofibers were compared regarding their capacity to release the drug in a controlled way in *in vitro* conditions mimicking the *in vivo* environment. Finally the therapeutic efficiency of DOX delivered in the nanosystems developed was evaluated in a relevant colorectal cell line.

2 EXPERIMENTAL SECTION

2.1 MATERIALS

Doxorubicin hydrochloride (MW = 578.98 g.mol⁻¹) was obtained from Sigma Aldrich, USA, as well as PEO (MW = 300 000 Da). PCL (MW = 80 000 Da) was purchased from Sigma Aldrich, United Kingdom, and chitosan (MW = 200 000 Da) was obtained from Glentham Life Sciences, United Kingdom. All reagents and solvents used in this work are summarized in the Table 1.

Table 1 – Used reagents and solvents

Chemicals	Characteristics	Supplier
Acetic acid	MW = 60.05 g.mol ⁻¹ (≥ 99.8 %)	E. Merck, Darmstadt, Germany
Boric acid	MW = 61.83 g.mol ⁻¹ (500 g)	Sigma Aldrich, USA
Chitosan	MW = 200 000 g.mol ⁻¹ (250 g)	Glentham Life Sciences, United Kingdom
Chloroform	MW = 119.38 g.mol ⁻¹ (≥ 99.5 %)	Alfa Aesar GmbH & Co KG, Germany
Citric acid	MW = 210.14 g.mol ⁻¹ (500 g)	Sigma Aldrich, USA
Doxorubicin hydrochloride	MW = 578.98 g.mol ⁻¹ (200 mg)	Sigma Aldrich, USA
Methanol	MW = 32.04 g.mol ⁻¹ (≥ 99.8 %)	Merck kGAa, 64271 Darmstadt, Germany
Poly(ethylene oxide)	MW = 300 000 g.mol ⁻¹ (500 g)	Sigma Aldrich, USA
Poly (ε-caprolactone)	MW = 80 000 g.mol ⁻¹ (250 g)	Sigma Aldrich, United Kingdom
Sodium phosphate decahydrate	MW = 380.12 g.mol ⁻¹ (1kg)	Sigma Aldrich, Germany
Sodium lauryl sulfate	MW = 288.372 g.mol ⁻¹ (500 g)	BDH Chemicals Ltd, England
Sulforhodamine B	MW = 558.666 g.mol ⁻¹ (1 g)	Sigma Aldrich, Germany

2.2 PREPARATION OF POLYMERIC SOLUTIONS

Two types of polymers, PEO and PCL, were chosen to produce polymeric nanofibers. PEO polymeric solutions were prepared by dissolving the polymer in water (0.104 g.mL^{-1}). To prepare PEO polymeric solution containing DOX, 1.75 wt% of DOX was dissolved in water and the polymer was slowly added to this aqueous solution containing the drug. For the preparation of PEO+CS polymeric solutions containing DOX, 0.70 wt%, 1.75 wt% and 3.51 wt% of CS were dissolved in 0.5 mL of acetic acid (90%) and then added to the PEO+DOX aqueous solution. PCL polymeric solutions were prepared by dissolving the polymer in chloroform:methanol (5:1) (0.12 g.mL^{-1}). To prepare PCL polymeric solution containing DOX, the drug was dissolved in chloroform:methanol at different concentrations: 1.39 wt%, 2.78 wt%, 5.56 wt% and 8.33 wt% and then the polymer was slowly added to this solution containing the drug. All polymeric solutions were kept under constant stirring at room temperature to ensure complete dissolution of the polymers and to obtain homogeneous solutions.

Preparation conditions of the polymeric solutions used in this study are summarized in Table 2.

Table 2 – Polymeric solutions used in the production of eletrospun nanofibers

Solutions	Polymer	Solvent	Drug
1	0.570 g PEO	5.5 mL water	–
2	0.570 g PEO	5.5 mL water	0.01 g DOX (1.75 wt%)
3	0.566 g PEO + 0.004 g CS (0.70 wt%)	5.0 mL water + 0.5 mL acetic acid (90%)	0.01 g DOX (1.75 wt%)
4	0.560 g PEO + 0.01 g CS (1.75 wt%)	5.0 mL water + 0.5 mL acetic acid (90%)	0.01 g DOX (1.75 wt%)
5	0.550 g PEO + 0.02 g CS (3.51 wt%)	5.0 mL water + 0.5 mL acetic acid (90%)	0.01 g DOX (1.75 wt%)
6	0.720 g PCL	6.0 mL chloroform:methanol (5:1)	–
7	0.720 g PCL	6.0 mL chloroform:methanol (5:1)	0.01 g DOX (1.39 wt%)
8	0.720 g PCL	6.0 mL chloroform:methanol (5:1)	0.02 g DOX (2.78 wt%)

9	0.720 g PCL	6.0 mL chloroform:methanol (5:1)	0.04 g DOX (5.56 wt%)
10	0.720 g PCL	6.0 mL chloroform:methanol (5:1)	0.06 g DOX (8.33 wt%)

2.3 PRODUCTION OF THE NANOFIBERS BY ELECTROSPINNING

Electrospinning is a process based on the formation of nanofibers by elongation of an electrically charged jet from a viscoelastic polymeric solution, through electrostatic forces [36, 61]. The photographic image and schematic setup of the electrospinning equipment used in this study are shown in Figure 5. The electrospinning setup was homemade at the Physics Department of University of Minho – Braga and includes a high voltage source, a syringe (containing the polymeric solution) terminating in a small diameter metal needle and a collector.

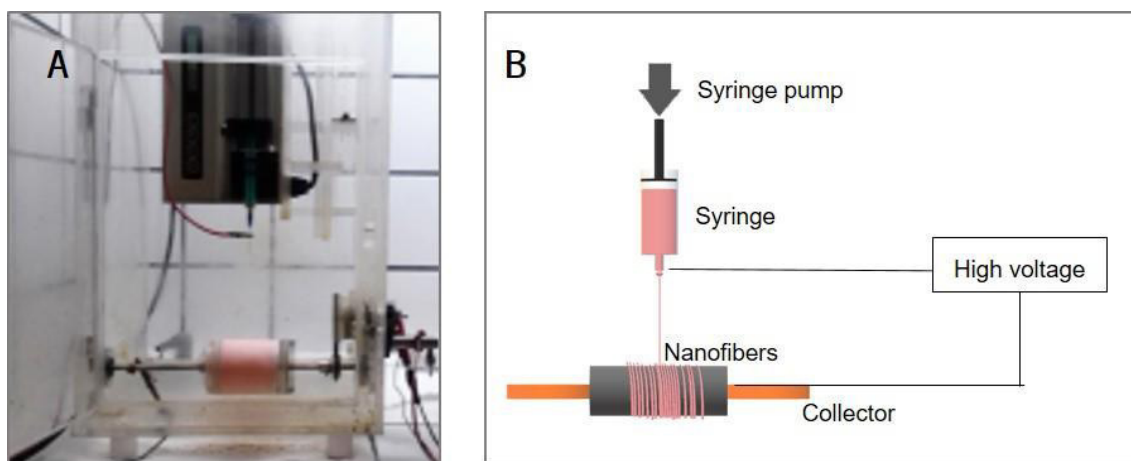


Figure 5– (A) Photographic image of homemade electrospinning setup
(B) Schematic illustration of the electrospinning setup

Initially a constant pressure is applied to the syringe containing the polymeric solution, which is at a fixed distance from the collector. This pressure pushes the solution to the tip of the needle where a drop of polymeric solution, with a certain surface tension, is formed. When this drop is subjected to an intense electric field (potential difference between the tip of the needle and the collector in the order of kV), positive charges are induced on its surface. The repulsion between the charges gives rise to a force opposite to the surface tension of the liquid. As the intensity of the electric field increases, the surface hemisphere of the liquid at the tip of the capillary elongates, forming a conical structure called the Taylor cone. When the electric field is higher than the repulsion value between the charges, it exceeds the critical value of the polymer surface tension

and the polymeric solution is ejected from the tip of the needle, towards the collector while the evaporation of the solvent occurs in the path between the tip of the needle and the collector [62].

For the production of PEO nanofibers a voltage of 20 kV, a flow rate of 0.03 mL.h⁻¹ and a needle with an inner diameter of 0.6 mm were used. These electrospinning parameters were kept for the production of PEO+DOX nanofibers and PEO+DOX+CS nanofibers.

For the production of PCL and PCL+DOX nanofibers a voltage of 15 kV, a flow rate of 0.6 mL.h⁻¹ and a needle with an inner diameter of 0.6 mm were used. In all cases, the distance between the tip of the needle and the collector was 12 cm. All the electrospinning parameters were kept constant and all the experiments were conducted at 18-22°C.

2.4 CHARACTERIZATION OF THE POLYMERIC NANOFIBERS

A variety of methods are used to characterize nanofibers and nanofibrous constructs after production and drug loading and most of these methods of characterization are not unique to nanofibers. The following methods were chosen to provide a comprehensive characterization of the nanofibers regarding important aspects such as topography and morphology, crystalline structure and thermic behavior, mechanical properties, chemical composition and surface properties.

2.4.1 Topographic and morphologic characterization

The surface topography, morphology and diameters distribution of the electrospun nanofibers produced were evaluated by scanning electron microscopy (SEM). SEM images were obtained on a Phenom ProX equipment (Paralab, Portugal). The analysis was done using the backscattered electrons detector (BSD) and an incident electron beam with an accelerating voltage of 15 kV. Samples were mounted on metal stubs using double-sided adhesive tape and were analyzed under low vacuum conditions, thus avoiding any additional coating step that is usually required when analyzing non-conductive samples. An image analysis software, Digimizer® (version 4.6.1, MedCalc Software), was used to acquire manual and accurate measurements of nanofibers diameters. The average diameter and diameter distribution of nanofibers were estimated upon analysis of 1000 random nanofibers taken from different areas of the mat and from different SEM images with 4000x magnification scale and were represented as a histogram plot. SEM was also used to measure the thickness of PCL nanofiber mat, as well as to estimate the nanofibers porosity, by the following equation

$$porosity = 1 - \frac{\rho_{apparent}}{\rho_{PCL}}$$

where ρ_{PCL} is the density of PCL ($\rho_{PCL} = 1.145 \text{ g cm}^{-3}$ as indicated by the supplier) and $\rho_{apparent}$ is the apparent density of the fiber mats, calculated from the mass to volume ratio of samples with a known surface area. To measure the thickness of the nanofibers mat, before cutting the fiber, the sample was immersed in liquid nitrogen to avoid distortion in the margin of the cut. Then the sample was mounted perpendicularly to the incident beam in order to access to the cut face of the sample.

2.4.2 Crystalline structure and thermic behavior

The structural characteristics of nanofibers were determined by X-ray diffraction (XRD). XRD patterns were recorded using a Philips Diffractometer, model PW1710 (Departamento de Ciências da Terra da Universidade do Minho, Braga) using incident radiation from $\text{CuK}\alpha$ ($\lambda = 1.54 \text{ \AA}$), current of 30 mA, voltage of 40 kV. Scans were carried out from 2.00° to 60.00° (2θ) at a scan rate of $2^\circ \cdot \text{min}^{-1}$.

In addition to the polymer crystallinity properties, the electrospun nanofibers were characterized regarding the thermic transitions suffered when the nanofibers are subjected to a temperature scan. This permits inferring about changes in endothermic or exothermic energy transitions in the polymeric matrices when the drug was incorporated in it. This thermal analysis was performed by differential scanning calorimetry (DSC) in a DSC 3+ Mettler Toledo analyzer under nitrogen atmosphere (flow rate of $20 \text{ mL} \cdot \text{min}^{-1}$). Samples were carefully weighed and sealed in aluminum pans and heated from 20°C to 100°C at a scanning rate of $10^\circ\text{C} \cdot \text{min}^{-1}$, in two cycles, in order to prevent thermal memory effect.

2.4.3 Mechanical properties

The mechanical behavior of the nanofibers was studied by carrying out stress-strain tests using an AGS-X Shimadzu 500N equipment (Departamento de Física da Universidade do Minho, Braga) with a 10 N load cell and a speed of $10 \text{ mm} \cdot \text{min}^{-1}$ at room temperature. The results were recorded as % of nanofibers elongation as a function of the applied stress.

2.4.4 Chemical composition

Throughout the present work it was essential to assess the chemical composition of the nanofibers with or without DOX to make proof of the successful drug encapsulation. The chemical composition evaluation was also necessary to evaluate interactions established between the drug and components of the nanofibers and to understand the effect of these interactions in DOX molecular integrity. For the purpose of chemical composition analysis two techniques were used, attenuated total reflectance Fourier transform infrared spectroscopy (ATR-FTIR) and nuclear magnetic resonance (NMR).

The infrared spectroscopy is used for characterization of chemical composition because each molecule absorbs specific energies that are associated to their characteristic bond-vibrations. When the frequency of the infrared beam light source is the same as the vibrational frequency of a bond, absorption occurs. Therefore, an infrared spectrum represents a fingerprint of a sample with absorption peaks that correspond to the frequencies of vibrations between the bonds of the atoms that are components of the material. The infrared absorption spectra were measured using a Fourier transform infrared spectrophotometer (Perkin-Elmer, Spectrum Two Spectrometer) equipped with an attenuated total reflection unit using a diamond crystal (Departamento de Biologia da Universidade do Minho, Braga). ATR-FTIR is a very suitable technique for solid samples because they can be simply placed on top of the crystal and do not require any previous preparation. Scanning range was made from 400 and 4000 cm^{-1} with increments of 4 cm^{-1} and each spectrum presented was an average of 16 scans.

In order to access how the chemical composition of DOX was affected by different environments, nuclear magnetic resonance (NMR) spectroscopy was used. This technique exploits the magnetic properties of certain atomic nuclei and so, indirectly, of the atoms and molecules in which they are contained. All isotopes that contain an odd number of protons and/or neutrons have a nonzero spin i.e. have an intrinsic magnetic moment and angular momentum. These isotopes, placed under the influence of a constant magnetic field, are polarized (aligned). This alignment can be disturbed by incident pulsed radiation in the range of the radiofrequencies, giving rise to peaks not only characteristics of each atom, but also of its vicinity. This phenomenon, called nuclear magnetic resonance, can therefore provide detailed information about the structure, dynamics, reaction state, and chemical environment of molecules. Samples were prepared by dissolution in deuterated water and transference into NMR capillaries. The NMR spectra was

measured in a Bruker Avance III 400, in which the ^1H frequency is 400.13 MHz and the external magnetic field is 9.4 T (Departamento de Química da Universidade do Minho, Braga).

2.4.5 Surface properties characterization

The characterization of the surface properties of the nanofibers is extremely important since the hydrophilic/hydrophobic character of the surface influences significantly the interaction between the nanofiber and the living tissues.

Contact angles of water on the surface of electrospun nanofibers were measured on a Drop Shape Analysis System DSA100 (Departamento de Física da Universidade do Minho, Braga) equipped with a CCD camera. In each measurement, deionized water was dropped onto the nanofiber sample from a needle of a microsyringe and images were taken a few seconds after the drop was set onto the sample surface. From these images, contact angle values were calculated.

2.5 EVALUATION OF THE POLYMERIC NANOFIBERS THERAPEUTIC PERFORMANCE

The therapeutic performance of the polymeric nanofibers developed is dependent on the capacity of these nanofibers to release their drug cargo in the biological media, as well as, their capacity to deliver an active form of the drug, that is still able to kill cancer cells. In this context two *in vitro* studies were performed, control release assays under biological mimetic conditions and cytotoxicity studies in a relevant cancer cell line.

2.5.1 Control release assays under biological mimetic conditions

For the control-released studies, a sample of the nanofiber mat was cut, weighted and exposed to the release medium. The release medium was a buffer solution with $\text{pH} \approx 5.5$ (pH of cancer cells tissue) or a micellar solution (sodium lauryl sulfate 16 mM which is a concentration well above the cmc) with adjusted $\text{pH} \approx 5.5$ to mimic not only the pH value of the cancer cells tissue but also its membranous/aqueous environment. The volume of release medium was always adjusted to guarantee sink conditions. All studies were carried out at 37°C under constant stirring at 80 rpm. In some tests the fibers mats were put directly in contact with the release medium while in other tests they were put into a dialysis bag with a cut-off of 3.5 kDa. In all experiments, aliquots of 1 mL of the released medium were taken at predetermined time points, while an equal amount

of fresh medium was added back. All the DOX release experiments were repeated at least twice. The amount of DOX released at each time point was quantified by UV-VIS spectroscopy in a Shimadzu UV-2501 PC spectrophotometer (Departamento de Física da Universidade do Minho, Braga). The measured absorbance of each sample, at $\lambda = 482$ nm, was converted in DOX concentration by means of a calibration curve. Then the cumulative amount of DOX released and the corresponding percentage relative to the maximum value were calculated and represented as a function of time.

2.5.2 Cytotoxicity studies in a relevant cancer cell line

The cell toxicology assays were done in human colorectal cancer cell line HCT-116 using the SRB (sulforhodamine B) method. This method is based on the property of SRB, which binds stoichiometrically to proteins under mild acidic conditions and then can be extracted using basic conditions. The amount of dye bonded to proteins can be used to estimate cell mass, which can then be used to estimate the cell viability.

A 24-well plate was used. HCT-116 cells (1×10^6 cells.mL⁻¹) were inoculated to each well containing the suitable nutrient cell medium (Dulbecco's Modified Eagle Medium-DMEM/F12) and incubated for 24 hours to allow the adherence of the cells to the wells. Next, eight different situations (three replicas for each one) were conducted: (1) negative control where only HCT cells were added; (2) neat PEO nanofibers; (3) neat PCL nanofibers; (4) 1 μ M DOX solution; (5) 4 μ M DOX solution; (6) PEO+DOX nanofibers (adequate amount of fibers was weighed in order to obtain 1 μ M of DOX in solution); (7) PEO+DOX nanofibers (adequate amount of fibers was weighed in order to obtain 4 μ M of DOX in solution); (8) PCL+DOX nanofibers (adequate amount of fibers was weighed in order to obtain 4 μ M of DOX in solution). After 48 hours of this treatment, the wells were washed with PBS buffer and a cell fixation solution (acetic acid 1% (v/v) in methanol) was added. After discarding the cell fixation solution and drying, 250 μ L of SRB solution (sulforhodamine B 0.5% (wt/v)) was added to each well and the plate was incubated at 37°C for 1h30 in the dark. The wells were washed again with 1% (v/v) of acetic acid to remove the unbound SRB and allowed to dry at 37°C for 10-15 min. Next, 1 mL of a 10 mM Tris solution at 4°C was added, in the dark, and stirred to dissolve the SRB bonded to the cell proteins. Finally, the absorbance of the dye (SRB) in each well was read at 570 nm in a microplate spectrophotometer (SpectraMax Plus 384, Departamento de Biologia da Universidade do Minho) in order to infer about

cell viability. 100% of cellular viability is attributed to the absorbance value obtained for the untreated cells (1) and the viability of the other wells is calculated considering this reference value.

3 RESULTS AND DISCUSSION

3.1 TOPOGRAPHIC AND MORPHOLOGIC CHARACTERIZATION OF PEO AND PCL NANOFIBERS

The SEM images of DOX (1.75 wt%) loaded PEO and PCL nanofibers are shown in Figure 6A and Figure 7A respectively. As expected, the nanofibers are randomly oriented due to the use of a slow rate rotating collector. In each figure, it is also presented the histogram of the nanofibers diameter distribution (Figure 6B and Figure 7B). The average diameter of PCL nanofibers (760 ± 300 nm) is larger than the average diameter of PEO nanofibers (340 ± 115 nm), which is the result of the electrospinning conditions established for the production of the nanofibers. Indeed, for the production of PEO nanofibers higher voltages and smaller flow rates were used.

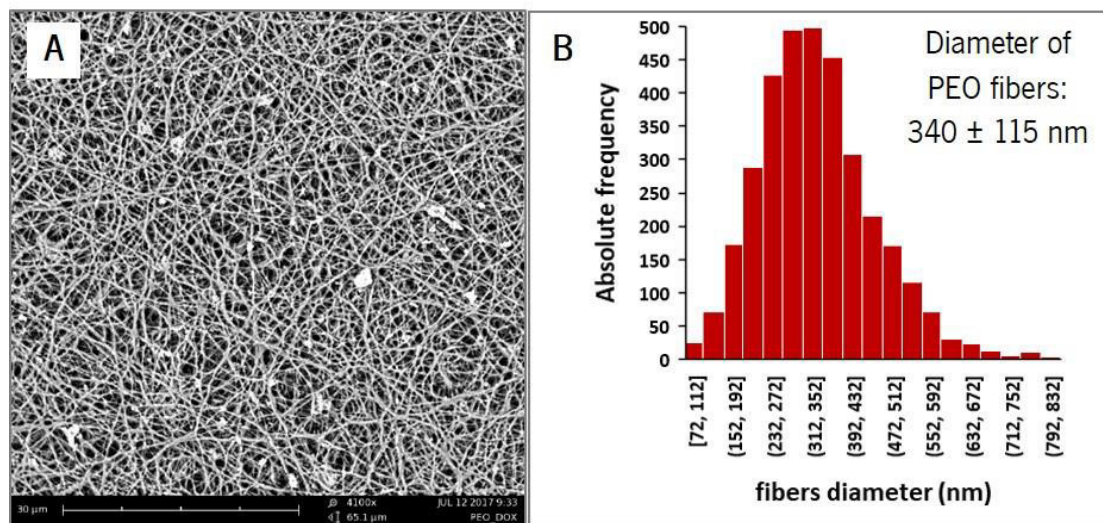


Figure 6 – SEM image of PEO nanofibers (4100x) and histogram of the diameters distribution of these fibers

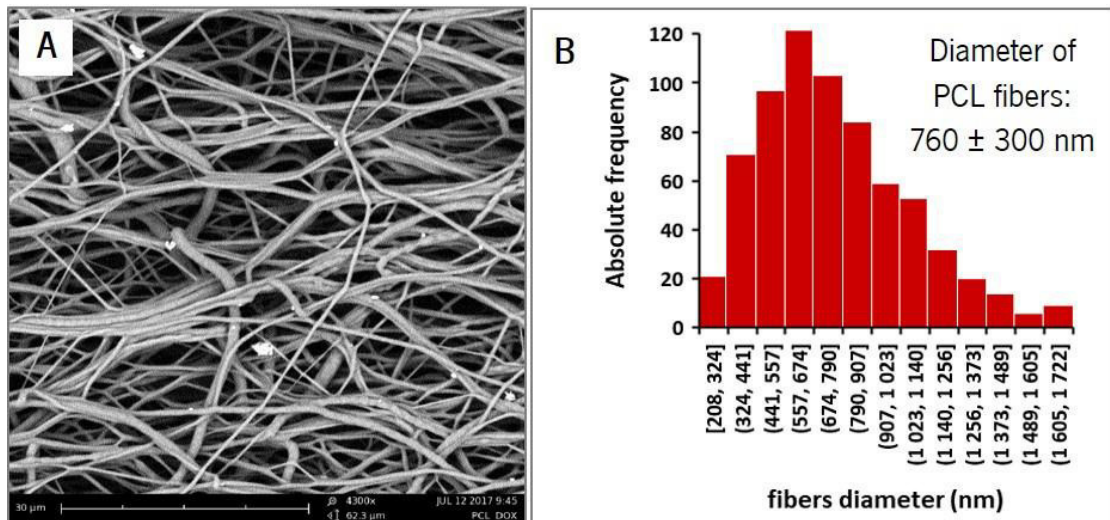


Figure 7– SEM image of PCL nanofibers (4100x) and histogram of the diameters distribution of these fibers

In order to estimate the porosity of the nanofibers, the thickness of a representative PCL fiber mat was measured (Figure 8). Using an average thickness of 315 μm, the calculated porosity was 0.74 indicating that about 74% of the nanofibers volume are voids. This high porosity turns these nanosystems into promising nanocarriers enabling high drug loading. This porosity value is in accordance with others published for typical nanofibers produced by electrospinning [63, 64].

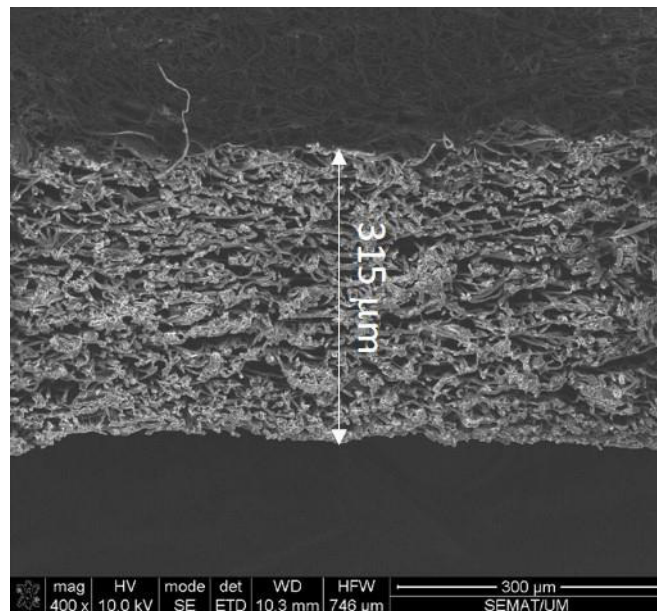


Figure 8– SEM image of a PCL mat, cut in liquid nitrogen, showing the thickness of the mat

3.2 CRYSTALLINE STRUCTURE AND THERMIC BEHAVIOR OF PEO AND PCL NANOFIBERS

In Figure 9, XRD spectra of DOX (1.75 wt%) loaded PEO and PCL nanofibers are represented. As shown, the crystalline structure of the polymeric nanofibers is not damaged by DOX encapsulation. Additionally, it is possible to assign small peaks probably due to the presence of the drug, such as the ones located at around 2θ of 17.0° and 14.5° .

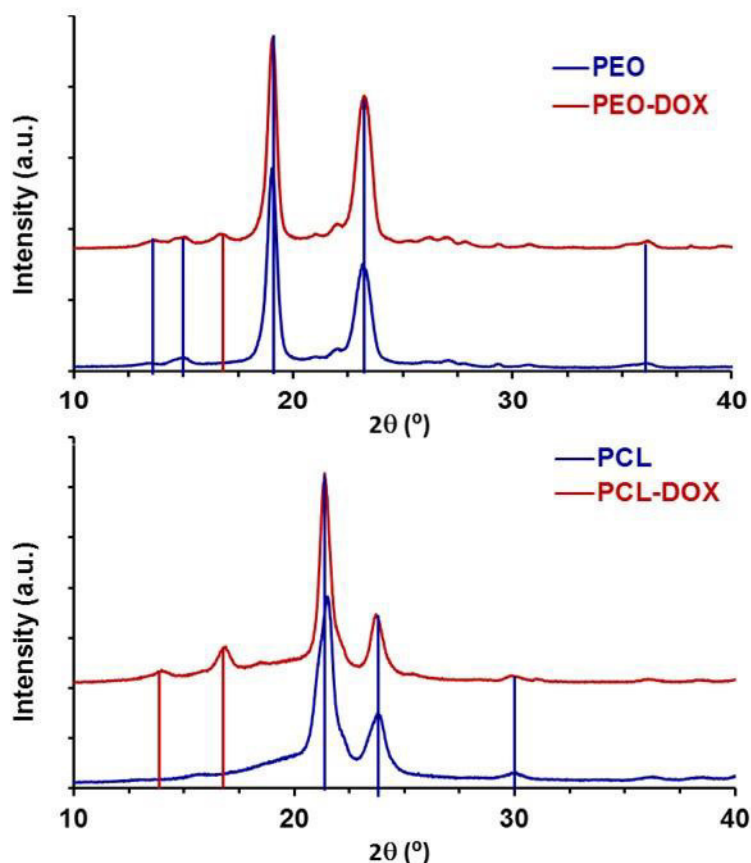


Figure 9 - XRD spectra of polymer nanofibers (PEO and PCL) without and with DOX encapsulation (blue lines are peaks assigned to the polymer while red lines are possible DOX peaks)

In Figure 10 differential scanning calorimetric (DSC) curves for PEO and PCL nanofibers without and with DOX (1.75 wt%) incorporation are shown. Neat nanofibers present the characteristic melting peaks of each polymer, at around 63°C for PCL [65] and around 58°C for PEO [66, 67]. For the DOX loaded nanofibers there is a broadening of the melting peaks to higher temperatures, which is in agreement with the rigidifying effect of the drug observed from the stress-strain assays (see section 3.3). Besides the broadening effect, the total energy necessary for the melting is reduced indicating that the drug incorporation induces a loss of crystallinity in the

polymeric nanofibers of about 11%, being the loss of crystallinity = $(\Delta H_{\text{nanofibers}} - \Delta H_{\text{nanofibers with DOX}})/\Delta H_{\text{nanofibers}}$. The small loss of crystallinity induced by the drug incorporation in the polymeric matrix corroborates the XRD studies which show no damage in the polymeric crystalline structure by drug incorporation. In the temperature range of this assay, DOX does not exhibit any thermic transition. The endothermic DOX transition occurs only at about 166.5°C [68].

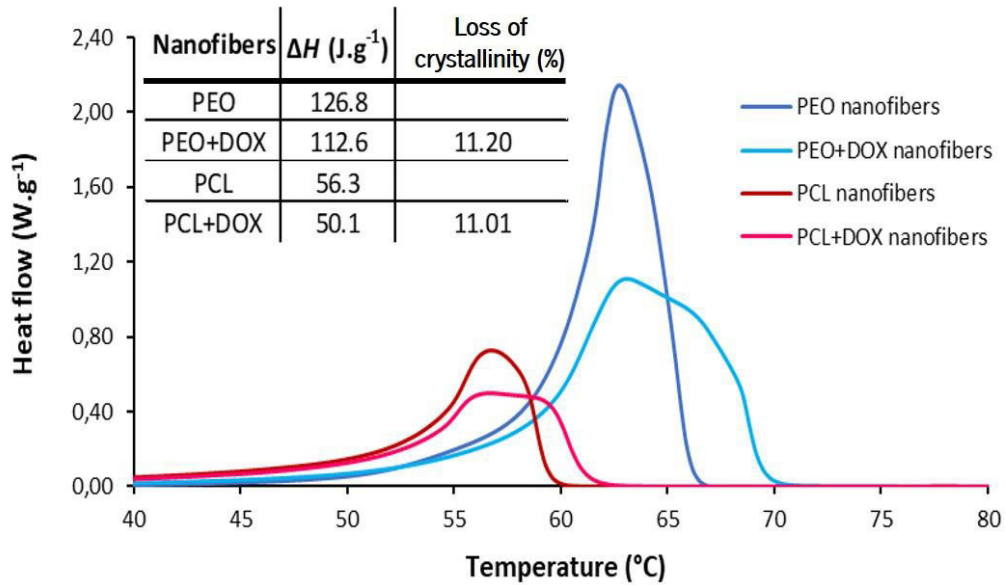


Figure 10 - DSC curves for PCL and PEO nanofibers without and with DOX incorporation

3.3 MECHANICAL PROPERTIES OF PEO AND PCL NANOFIBERS

Figure 11 shows the stress-strain curve for the produced polymeric nanofibers. Elongation was measured versus applied force. In order to take the measurement independent of the thickness of the fiber, stress, σ , was calculated by dividing the applied force by the fiber section. Strain is the relative elongation, $\varepsilon = \Delta L/L_0$ where L_0 the initial length of the fiber.

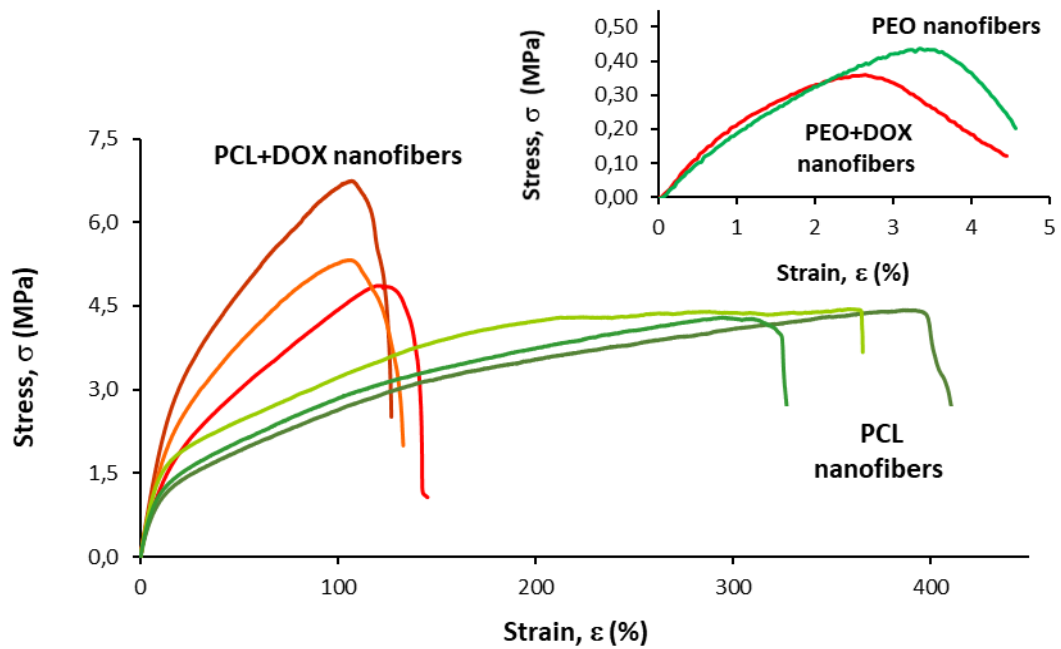


Figure 11– Stress-strain curve for PCL and PEO fibers without and with DOX incorporation

PCL nanofibers are incomparably more resilient and elastic than PEO nanofibers. It is further noted that, in agreement with the results obtained in DSC measurements (see section 3.2), the encapsulation of the drug into the PCL fibers makes them more rigid. They support higher tensile strengths but break at lower elongation.

3.4 CHEMICAL COMPOSITION OF PEO AND PCL NANOFIBERS

In Figure 12 and Figure 13, ATR-FTIR spectra of DOX (1.75 wt%) loaded PEO and DOX (8.33 wt%) loaded PCL nanofibers are depicted.

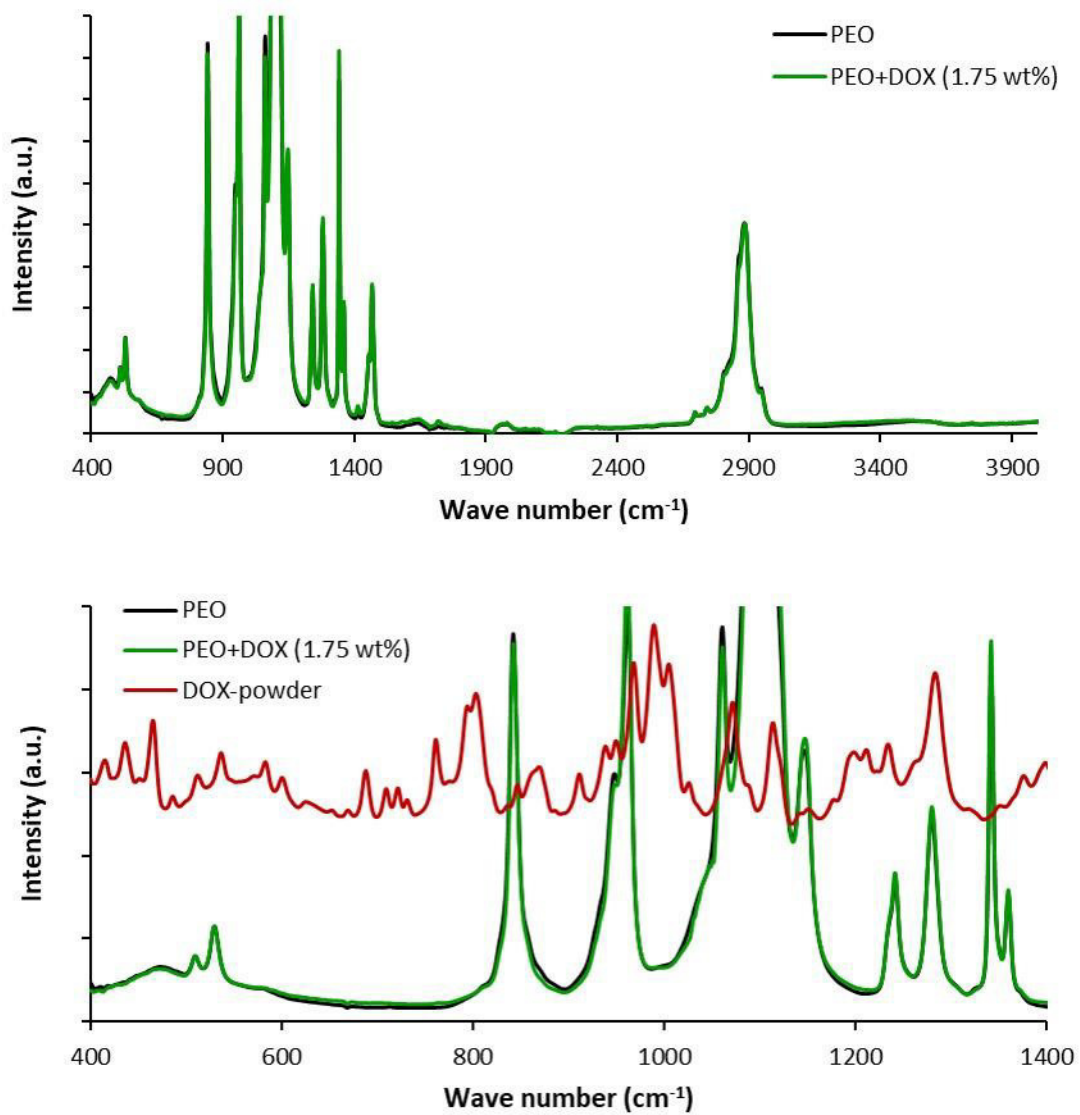


Figure 12 – ATR-FTIR spectra of PEO and PEO-DOX (1.75 wt%) nanofibers. Also shown, for comparison, ATR-FTIR spectra of DOX (powder)

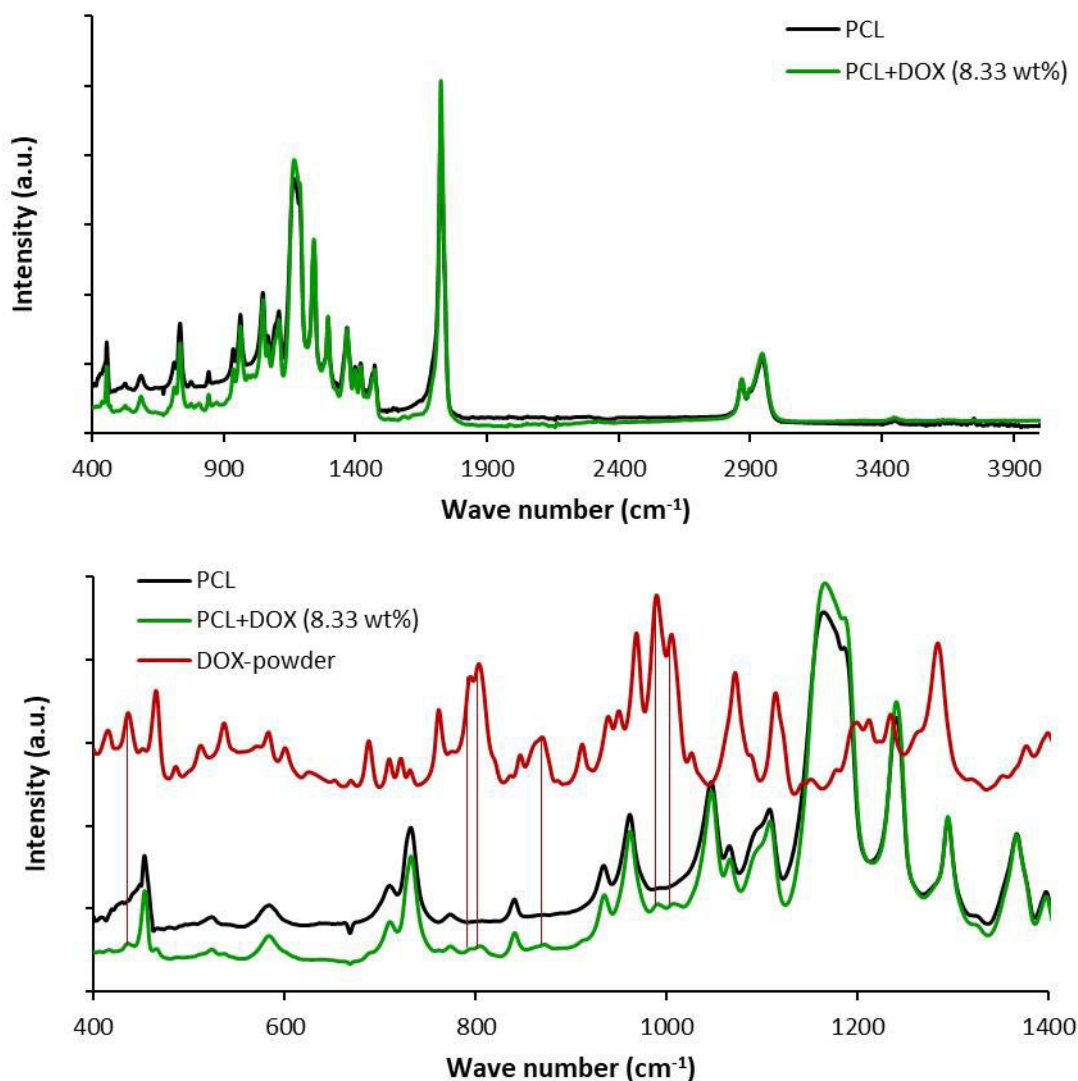


Figure 13 – ATR-FTIR spectra of PCL and PCL-DOX (8.33 wt%) nanofibers. Also shown, for comparison, ATR-FTIR spectra of DOX (powder). Red lines identify bands attributed to DOX.

In agreement with the reported literature, PEO nanofibers exhibited the two most characteristic bands, one at 1107 cm^{-1} attributed to the C–O–C bond stretching vibration of the repeated $-\text{CH}_2-\text{O}-\text{CH}_2-$ units of poly(ethylene glycol) and the other one at $2940-2889\text{ cm}^{-1}$ assigned to C–H stretching bonds [41, 45]. PCL nanofibers also exhibited the three most characteristic bands reported in the literature [69, 70]: one, located at 1166 cm^{-1} , attributed to symmetric C–O–C bond stretching of the repeated monomers within the PCL polymer, another, very strong, located at 1723 cm^{-1} and resulting from carbonyl group bond stretching and at $2940-2860\text{ cm}^{-1}$ a broad band attributed to C–H stretching.

In the spectrum shown in Figure 12, DOX (1.75 wt%) loaded PEO, it was not possible to identify any bands attributed to the drug. Instead, for the DOX (8.33 wt%) loaded PCL some bands

(signalized in Figure 13 by red lines) can be clearly attributed to DOX [45, 71]. The band located at 870 cm^{-1} is attributed to the primary amine (NH_2) wagging and the bands located around $990\text{--}1000\text{ cm}^{-1}$ are also well identified in the literature.

3.5 SURFACE PROPERTIES CHARACTERIZATION OF PEO AND PCL NANOFIBERS

Young [72] expressed the contact angle θ_c of a water droplet on a flat solid surface by the following equation: $\cos \theta_c = (\gamma_{sv} - \gamma_{sl}) / \gamma_{lv}$, where γ_{sv} , γ_{sl} and γ_{lv} are the interfacial surface tensions of solid-vapor, solid-liquid and liquid-vapor interfaces, respectively. The forces created by surface tensions at each interface pull water drops in the solid plane and define its shape. Based on Young's definition, Figure 14 shows schematic views of different superhydrophilic, hydrophilic, hydrophobic, and superhydrophobic surfaces and respective water contact angles [73].

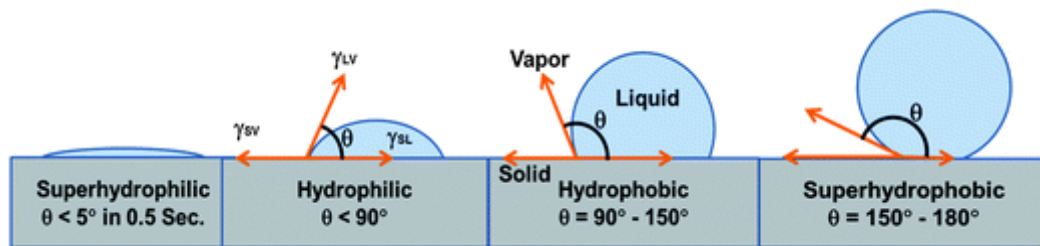


Figure 14– Schematic view of superhydrophilic, hydrophilic, hydrophobic, and superhydrophobic surfaces classifications according to the water contact angle. Adapted from [73]

The results of the contact angle measurements of PEO+DOX and PCL or PCL+DOX nanofibers are shown in Figure 15.

The contact angles of PEO nanofibers with DOX encapsulated were not possible to measure as the drop was immediately absorbed. In this case, the nanofiber is considered to have a superhydrophilic surface. Contrastingly, the contact angles of PCL nanofibers without or with DOX are all over 120° . The high contact angle clearly reveals the hydrophobic behavior of PCL nanofibers, which increases with DOX content. This phenomenon can be interpreted in terms of the effect that an additive, like a drug incorporated in the nanofiber, has on the chemical composition of the surface, but also on the roughness and surface area [73, 74]. Therefore, despite DOX being a drug with polar chemical groups, which would in principle favor an increase in

hydrophilicity, its deposition and insertion within the nanofibers matrix may generate instead additional roughness which explains the increase in hydrophobicity. This is actually in agreement with what has been described for additives that increase nanofibers hydrophobicity by an increase in roughness, which in turn causes loss of some mechanical properties [73]. Similarly, the inclusion of DOX in PCL nanofibers has also resulted in a rigidifying effect and loss of some mechanical properties as the drug loaded PCL fibers break at lower elongation than neat PCL nanofibers (see Figure 11).

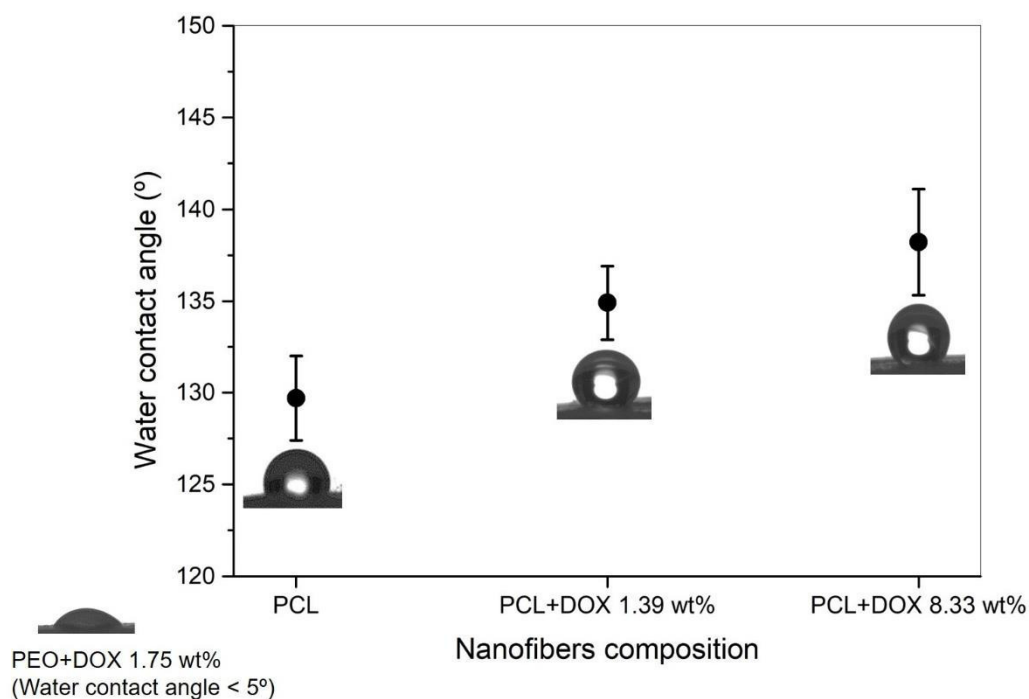


Figure 15– Water contact angles and corresponding shapes of water droplets for electrospun PEO and PCL nanofibrous mats in the absence and in presence of different DOX contents

3.6 EVALUATION OF THE PEO AND PCL NANOFIBERS THERAPEUTIC PERFORMANCE

3.6.1 Control release assays of DOX loaded PEO nanofibers under biological mimetic conditions

The control release assays of PEO nanofibers loaded with DOX (1.75 wt%) was made in a buffer medium (pH \approx 5.5) to simulate the physiological pH media of acidic tumor environments.

The nanofibers were put directly into the aqueous medium and the % of drug released in a time course is presented in Figure 16.

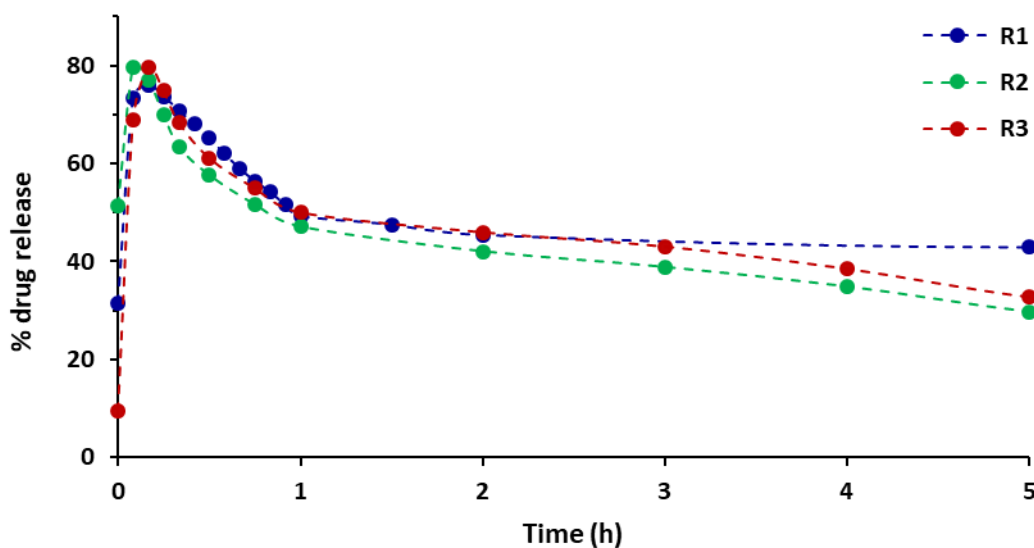


Figure 16 – Control release of PEO-DOX (1.75 wt%) nanofibers in buffer pH \approx 5.5 (three replicas). Dashed lines are only eye guides

The nanofiber mat dissolves immediately in the aqueous medium and after 10 minutes, DOX reaches the maximum concentration. It should be noted, however that the maximum concentration measured for the drug never reaches 100%. Additionally, it is observed that during the first hour of the assay the measured drug concentration decreases by almost 40%. This behavior of DOX in the presence of PEO will be further investigated.

To fulfill the aim of this work, develop a nanosystem able to deliver the drug in a controlled manner during larger periods of time, it was important to retard the dissolution of the nanofibers. Therefore, and after literature review, chitosan (CS) was chosen to be included in the nanofibers composition, since this polysaccharide can control the solubilization rate of aqueous soluble polymers, such as PEO [45, 53, 75, 76].

So, to avoid the fast dissolution of PEO nanofibers, increasing amounts of CS (0.70, 1.75 and 3.51 wt%) were included in the polymeric solutions (see Table 1). The drug release profiles obtained from PEO-CS-DOX (1.75 wt%) nanofibers in a buffer medium (pH \approx 5.5) are shown in Figure 17.

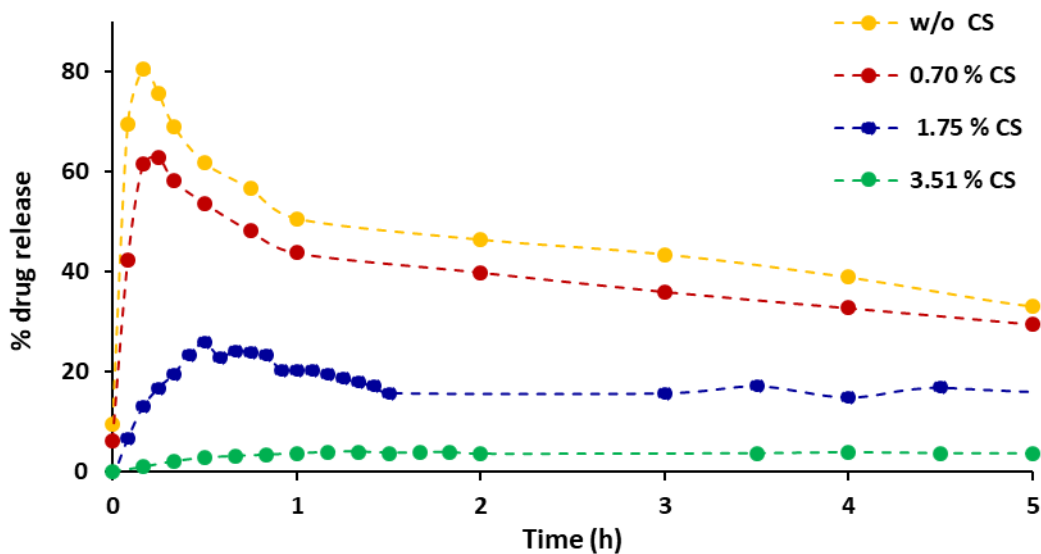


Figure 17– Control release of PEO–CS- DOX (1.75 wt%) nanofibers in buffer pH \approx 5.5 using three different CS content. Dashed lines are only eye guides

From Figure 17 it is possible to observe that the amount of DOX released decreases with the increase of CS concentration in the nanofiber. Furthermore, it was observable that the nanofibers with CS do not dissolve completely but disaggregate in small pieces and the ones with the highest CS concentration take longer to disaggregate. This suggests that CS forms a protecting shell preventing the dissolution of PEO-DOX nanofibers limiting the release of the drug. Indeed, in the literature core-shell nanofibers containing aqueous soluble polymers and CS are reported [45, 53, 75]. Using this approach, the release of DOX was delayed, however the maximum amount achieved was reduced with the increase of CS because the drug retained into the non-solubilized fibers was not released. Therefore, this did not seem to be a good strategy.

Thinking on the therapeutic application of these nanocarriers, chiral loci or colorectal cancer, another approach for the control release assays was considered. To mimic the reduced volumes of physiological fluids, the control release assays were performed confining the nanofiber mats in a dialysis bag. These results are shown in Figure 18.

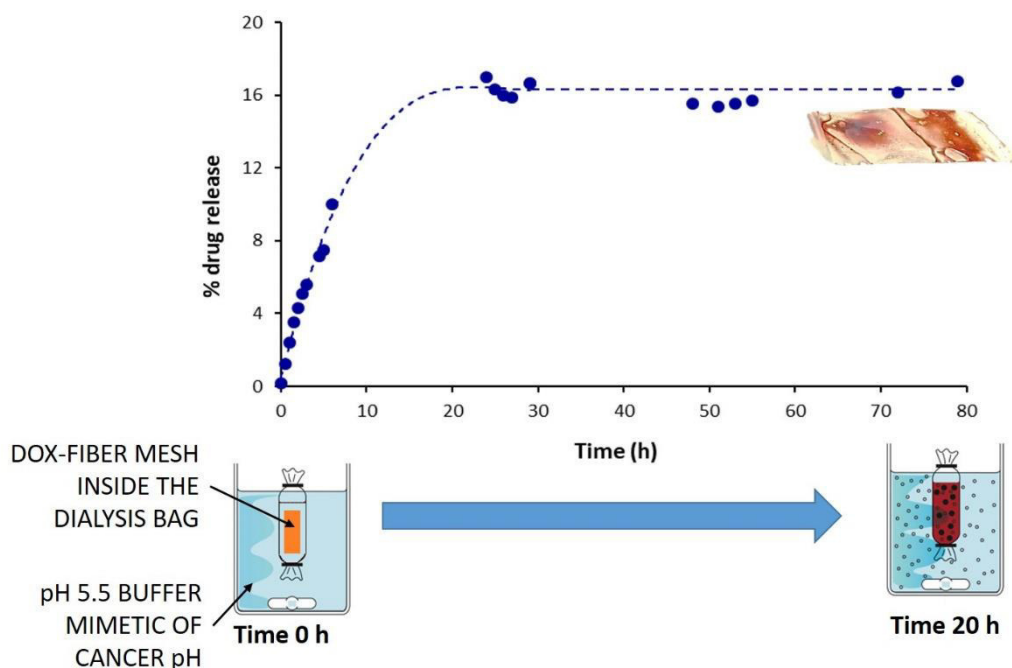


Figure 18 – Control release of PEO-DOX (1.75 wt%) nanofibers placed into a dialysis bag in buffer pH \approx 5.5. Also shown a photograph of the dialysis bag at the end of the assay. Dashed lines are only eye guides. The cartoon elucidates the procedure of control release assay in a dialysis bag.

As can be seen the drug is slowly released taking about 20 h to reach its maximum amount. Comparing with the previous assay (without the dialysis bag), the maximum amount of DOX in the release medium is much smaller (only about 16%) but does not decrease with time. At the end of the assay a suspension with a gel appearance is formed inside the dialysis bag (photo in Figure 18). This gel seems to contain the polymer and the most part of the drug. The retention of the polymer inside the dialysis bag justifies that the drug detected is kept constant with time. On the other hand, in the assays performed without the dialysis bag (Figure 16), the presence of both polymer and DOX in the release medium causes a great decrease on the detected drug (about 40% in the first hour). This behavior indicates that there must be an interaction between the drug and the polymer that promotes the hydrolysis of the anthracyclinone aromatic backbone of DOX, with consequent decrease of the absorbance detected. If that is the case, both PEO and PEO-CS nanofibers that promoted the decrease in DOX detected (Figure 16 and Figure 17), could be responsible for strong interactions with the drug resulting in its hydrolysis and consequent possible loss of therapeutic efficiency. To further explore this assumption the interactions between DOX and PEO or between DOX and PEO-CS were studied in different pH media and by different techniques (ATR-FTIR and RMN) that could elucidate about chemical changes in the drug molecule.

3.6.2 Stability studies of DOX in presence of PEO or PEO-CS

The stability of DOX in aqueous medium (pH 5.5), in the absence or in the presence of PEO, was evaluated (Figure 19).

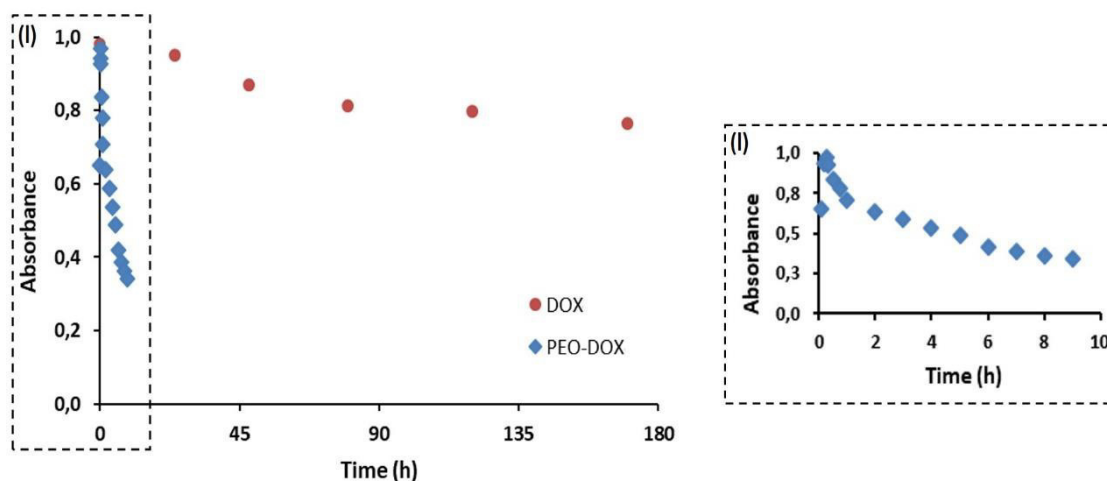


Figure 19 – Absorbance versus time for DOX and PEO-DOX in buffer solutions (pH \approx 5.5). Inset (I) shows in more detail the absorbance decrease of DOX in PEO-DOX buffered solutions for the first 9 hours.

In the literature several stability studies of DOX and other anthracycline derivatives have identified degradation products that are formed extensively in basic pH media and less extensively at low pH values and in non-aqueous media [77-79]. Accordingly, within the current study it was also observed that when DOX is alone in the aqueous medium (pH \approx 5.5), it suffers a small and slow hydrolysis, as observed by the decrease of the detected drug (of only about 20 % in one week) (Figure 19, red dots). However, when DOX is in the presence of PEO (Figure 19, blue dots), a much faster hydrolysis of the drug occurs as proved by the steep decrease of the drug absorbance that reaches about 40 % in the first hour and 65 % in 9 hours (Figure 19 (I)). Another observation that could be made is that PEO-DOX interaction and consequent DOX hydrolysis is pH dependent as it is very efficient in aqueous and slightly acidic medium (pH \approx 5.5), but it is prevented in strongly acidic medium. This is illustrated in Figure 20, where the control release results of PEO-DOX (1.75 wt%) nanofibers in aqueous buffer (pH \approx 5.5) and in acetic acid (90%) are shown.

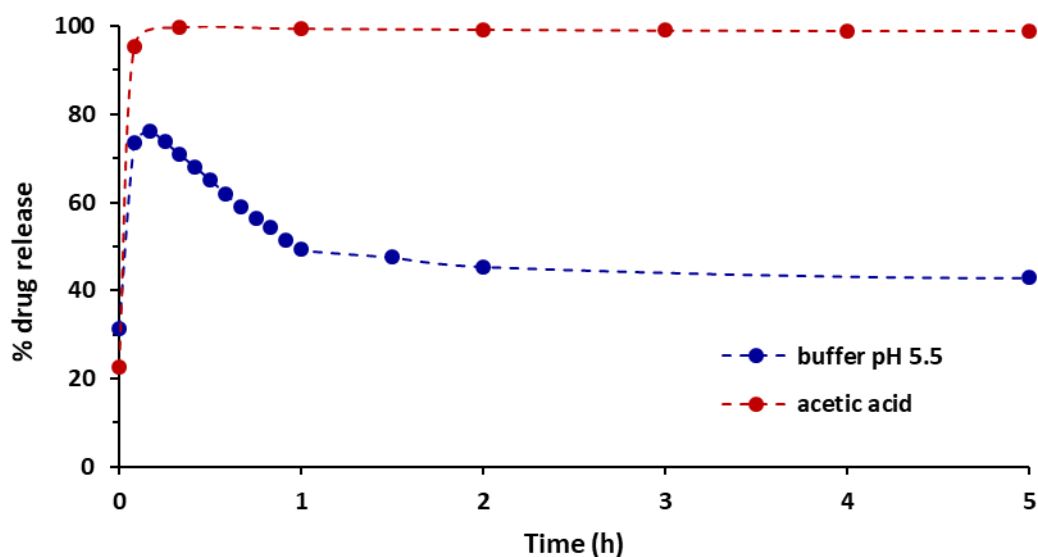


Figure 20– Control release of PEO-DOX (1.75 wt%) nanofibers in buffer pH \approx 5.5 and in acetic acid. Dashed lines are only eye guides

Although the mechanism by which DOX and PEO interact is not known with certainty at this point, it is possible to perceive from the literature that DOX interacts strongly with other polymers, such as polyethylene, polytetrafluoroethylene, polyvinylchloride [80-82]. On the other hand, PEO is also described as able to interact with numerous compounds by its capacity to establish hydrogen bonds [83, 84]. Furthermore, the interactions between PEO and other components are also described as pH dependent. Indeed, although the ability of PEO to act as hydrogen bond acceptor is unaffected by pH due to its non-ionic nature, the capacity of the hydrogen bond donor that binds to PEO may instead be pH dependent [83, 84]. This can be the case of DOX which for low pH values is protonated at the amino group and the repulsive force between positively charged groups is large enough to prevent the growth of the DOX-PEO assembly. When the pH increases from strong acidic to about 5.5, adsorption between DOX and PEO increases and a possible explanation is that neutral amino species of DOX increase with pH [79] and this neutral group has higher affinity to act as hydrogen bond donor to the ether group of PEO that act as hydrogen bond acceptor (Figure 21). The interaction established between DOX and PEO is possibly an initiation step for DOX molecular hydrolysis since in the literature the interaction of this drug with other polymers is also described as responsible for drug degradation [80-82].

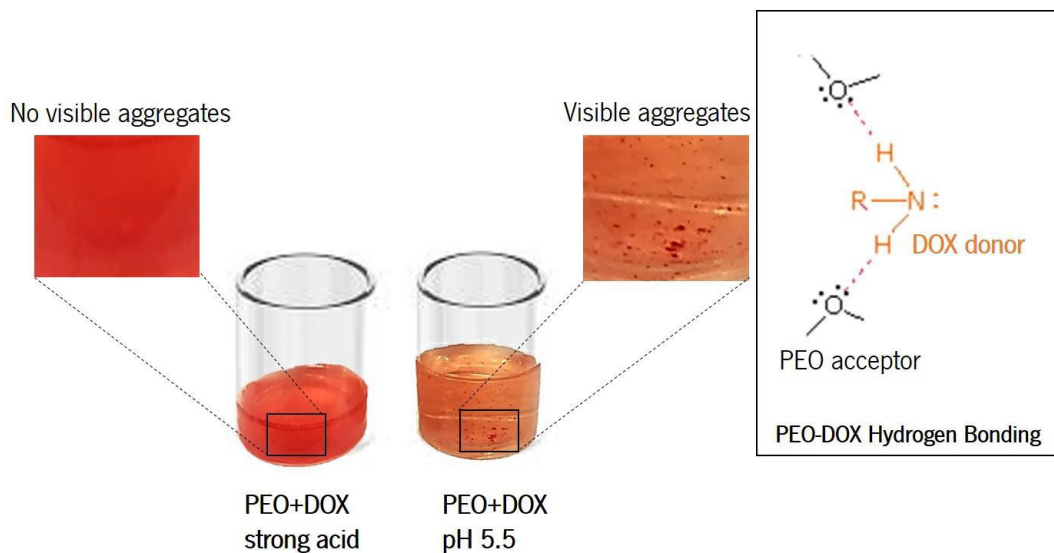


Figure 21– Solutions of PEO+DOX powders in buffer pH \approx 5.5 and in strong acid (acetic acid 90%) and representation of possible PEO-DOX interaction through hydrogen bonding

DOX hydrolysis after interacting with PEO was also evidenced by other techniques such as NMR and ATR-FTIR. The NMR spectra shown in Figure 22 were obtained from the medium (buffer pH \approx 5.5) where the control release assays of PEO-DOX and PEO-CS-DOX nanofibers were performed. The DOX and CS content were both 1.75 wt%. At the end of the control release assay, the aqueous medium was completely dried and then the solid residue was dissolved in deuterated water and analyzed by NMR. Note that, in Figure 22, the intense peak at 4.800 ppm arises from the deuterated water.

Figure 23 shows, in more detail, the 2-3 ppm chemical shift region which represents the most relevant region contributing with more than 98% of the NMR signal. The NMR spectra are similar although a displacement of about 0.5 ppm for smaller chemical shifts values is observed in the presence of CS.

In order to facilitate the interpretation of these spectra, the NMR spectra of DOX (powder) and of PEO (powder) in deuterated water are shown in Figure 24.

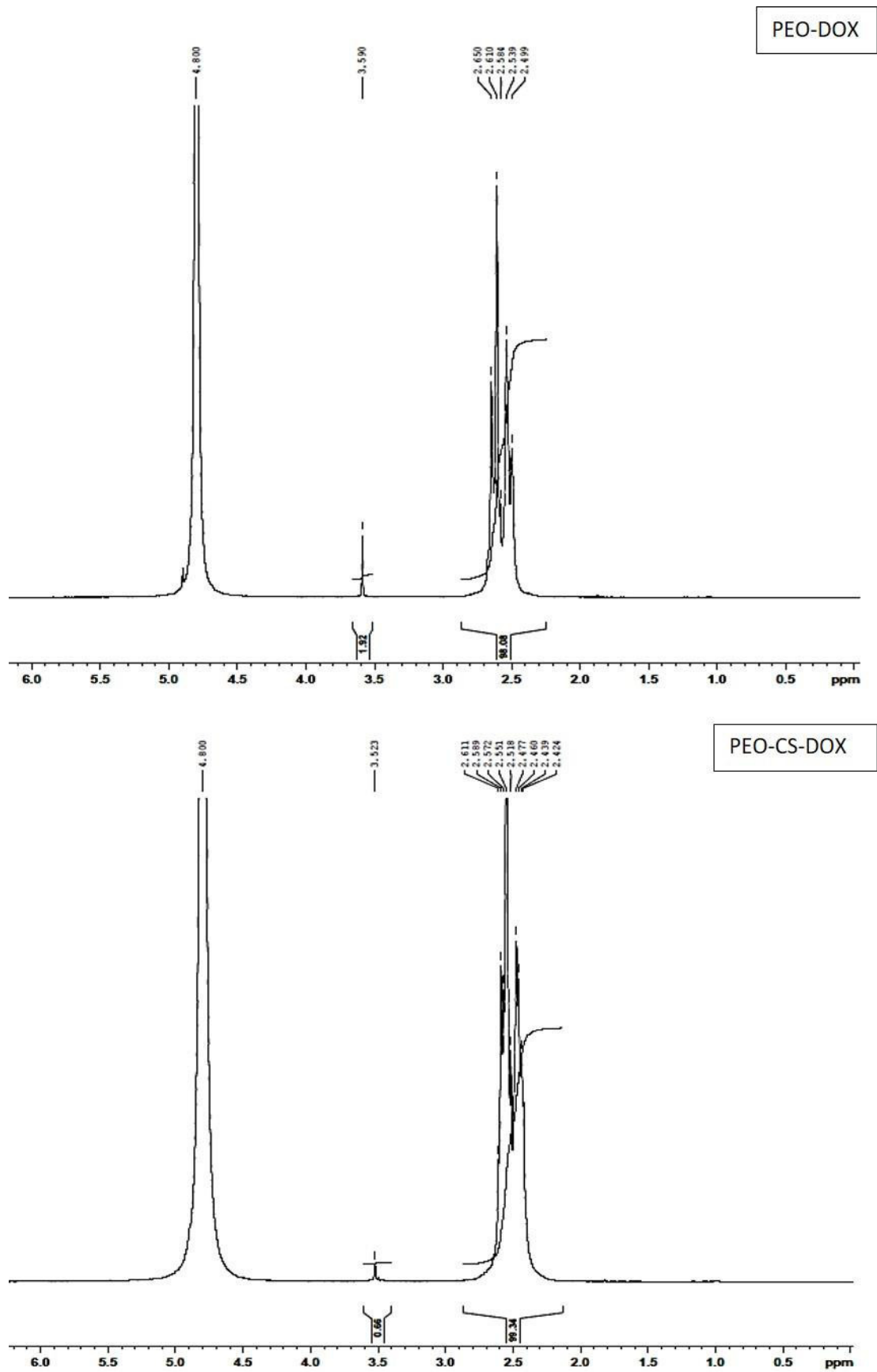


Figure 22 – NMR spectra of PEO-DOX and PEO-CS-DOX obtained from drying control release medium and posterior dissolution of residues in deuterated water.

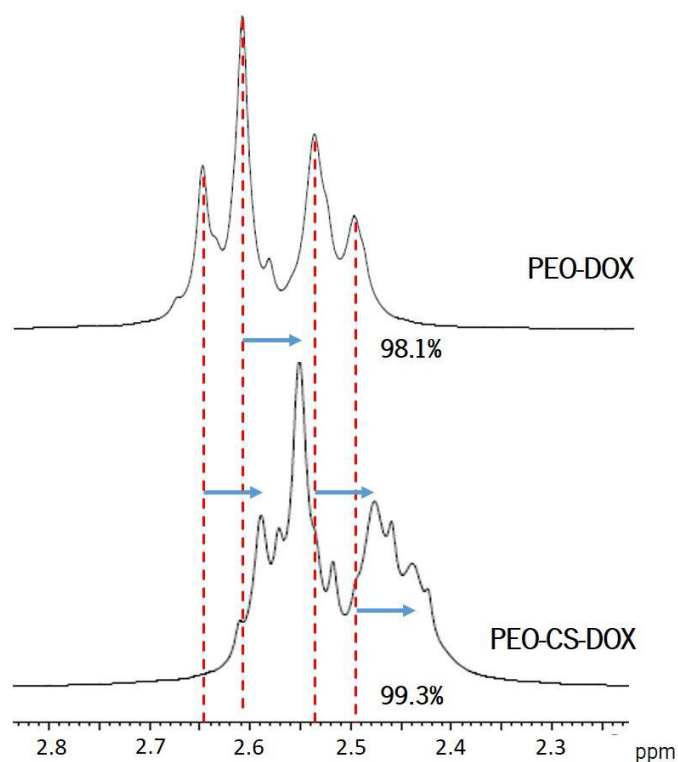


Figure 23– NMR spectra of PEO-DOX and PEO-CS-DOX obtained from drying control release medium and posterior dissolution of residues in deuterated water (detail of the 2-3 ppm region). Red dashed lines assign the location of NMR bands in PEO-DOX residues. These bands are shifted of about 0.5 ppm in PEO-CS-DOX residues (blue arrows indicate the shift).

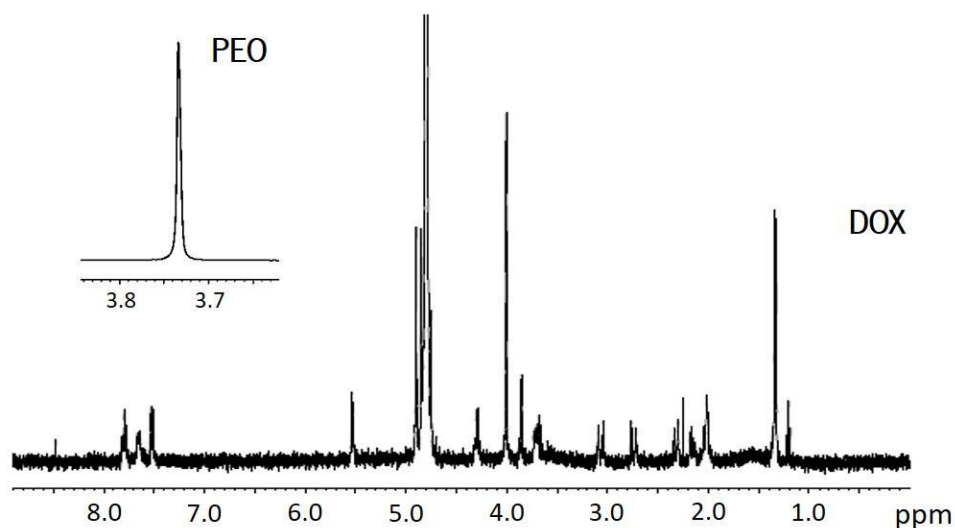


Figure 24 – NMR spectra of DOX (powder) and PEO (powder) in deuterated water.

It is observed that the NMR spectra of pure DOX (Figure 24) is much more complex than the NMR spectra of the drug when in presence of PEO or in presence of the polymer and CS (Figure

22). Indeed in the NMR spectra of control release residues (Figure 22) no peaks corresponding to the free DOX are observed and only a very small peak, located in 3.5-3.6 ppm, appears that can be attributed to PEO (see PEO NMR characteristic band in Figure 24). Furthermore, the set of peaks detected in Figure 23, with chemical shifts in the 2-3 ppm region, does not correspond to DOX chemical shifts (Figure 24). This indicates that upon interaction with PEO and PEO-CS there is a complete change in DOX chemical structure, which confirms the previously observed drug degradation, probably due to an efficient hydrolysis of DOX anthracycline aromatic backbone.

By ATR-FTIR it was also possible to confirm the presence of DOX degradation products resulting from its interaction with PEO. ATR-FTIR spectra shown in Figure 25 were obtained from drying the residual gel that remained inside the dialysis bag at the end of the control release assay. For comparison, ATR-FTIR spectra of DOX (powder) and PEO (nude nanofibers) were also shown in the same figure. Comparing these spectra with those of the nanofibers before the control release (see Figure 12) it can be concluded that a huge difference is observed. Before the control release, PEO-DOX nanofibers spectrum is similar to the nude PEO nanofibers spectrum. After the control release in aqueous medium, completely different spectra are obtained revealing the presence of new bonds probably due to the formation of PEO-DOX complexes with degradation of DOX aromatic ring.

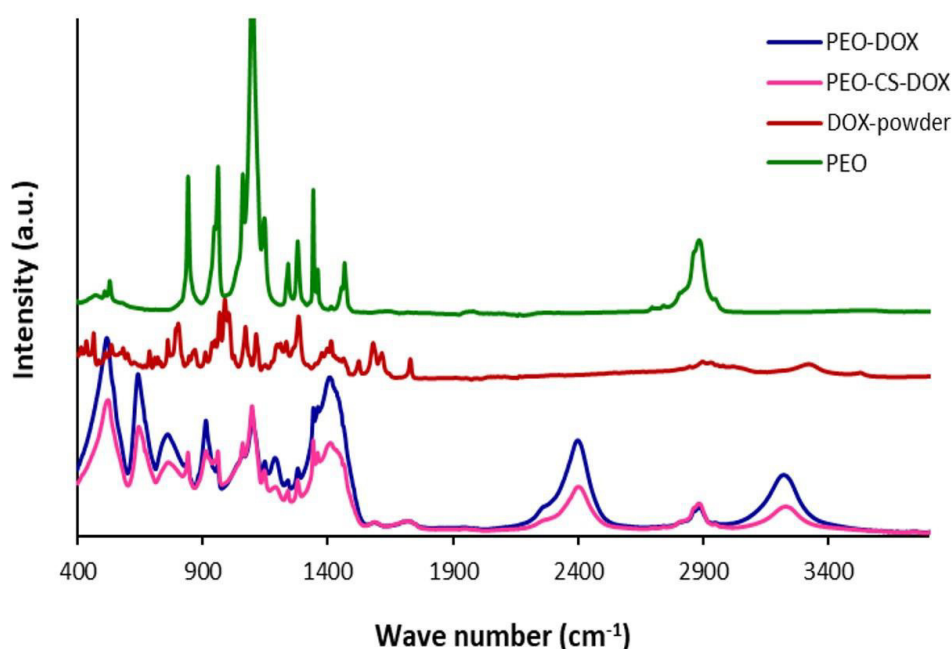


Figure 25 – ATR-FTIR spectra from the dried residual gels that remained inside the dialysis bag at the end of the control release assay of PEO-DOX and PEO-CS-DOX nanofibers. For comparison DOX (powder) and PEO (nude nanofibers) spectra are also shown.

Although the results obtained do not allow to fully understand the mechanism of DOX degradation, it is possible to infer that there is a lysis in the aromatic ring, shown by the decrease of the absorbance in the visible region. This loss of aromaticity will affect the planar structure of the molecule by preventing its intercalation in the DNA and therefore its therapeutic effect, as it will be confirmed by the cellular assays carried out (see section 3.6.4).

3.6.3 Control release assays of DOX loaded PCL nanofibers under biological mimetic conditions

To overcome the problems associated with the degradation of DOX in the presence of PEO, the drug was encapsulated in PCL nanofibers. These fibers are much stronger and much more elastic (see Figure 11). They are still biodegradable and biocompatible, being this polymer approved by FDA for human use and for drug delivery. *In vivo*, and in the presence of enzymes found in animal fluids, such as α -amylase and lipase, PCL degrades after a few weeks [85-87]. The main disadvantage of PCL nanofibers is their high hydrophobicity (contact angle about 130° as seen in Figure 15), making their wettability extremely low. Therefore, these fibers are not water-soluble as PEO nanofibers were.

The first control release assays were made by placing PCL nanofibers directly in contact with the aqueous medium (buffer pH \approx 5.5). The results obtained, for different drug loaded contents, are shown in Figure 26 and Figure 27.

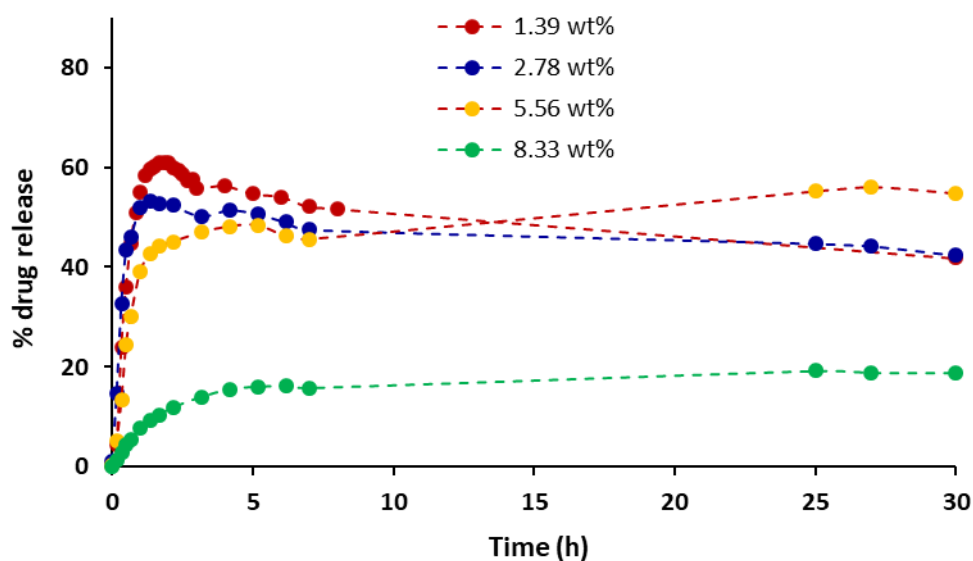


Figure 26 – Control release of PCL-DOX nanofibers in buffer pH \approx 5.5 using four different DOX content. Dashed lines are only eye guides.

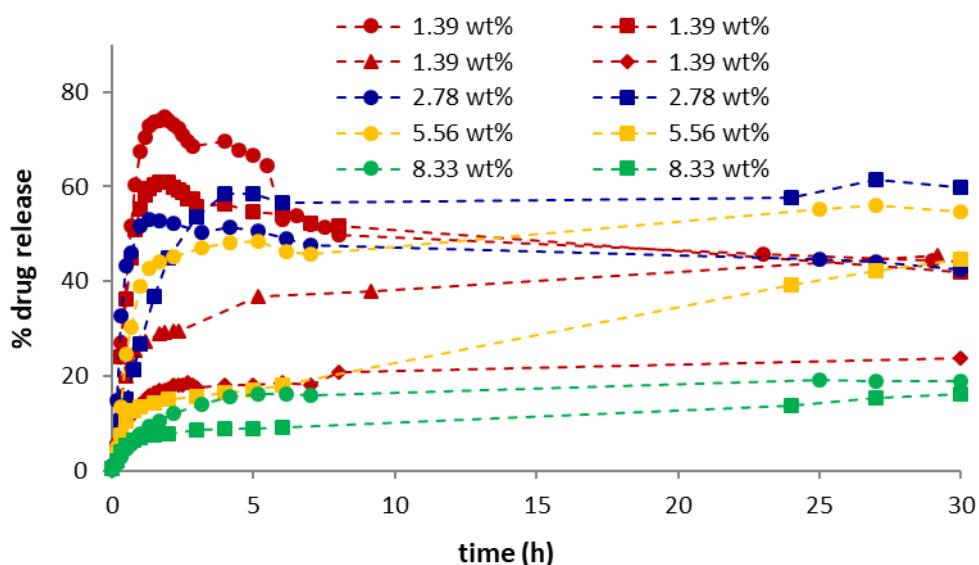


Figure 27– Control release of PCL-DOX nanofibers in buffer pH \approx 5.5 using four different DOX contents evidencing the great variability between replicas. Dashed lines are only eye guides.

These results justify some comments. First of all, it is worth to note the huge difficulty in wetting the fibers resulting in great differences between replicas as shown in Figure 27. The lack of wettability of either PCL or PCL+DOX nanofibers has been previously proved by contact angle measurements (see Figure 15). It is also clear that DOX is released from PCL nanofibers as soon as they are wetted. The results also seem to indicate that the nanofibers with higher DOX content have a slower release of DOX and the % of DOX released is the smallest comparing to nanofibers with smaller DOX content. This could be also due to the low wettability of the nanofibers. Indeed, PCL nanofibers with high DOX content have demonstrated to be more hydrophobic by contact angle measurements justifying the difficulty of these fibers to be wetted by the release medium, and consequently the difficulty of DOX to be released into the medium.

Furthermore, it is observed that the % of drug released never reaches 100%, indicating some kind of equilibrium between the drug concentration in the PCL nanofibers and in the aqueous medium. Looking at the release profile, a greater % of drug released is obtained in the early stages, but then it decreases reaching an equilibrium value. To confirm the assumption that an equilibrium is reached between the amount of DOX retained into PCL nanofibers and the amount of DOX released in the aqueous medium, after 2 hours of control release assay, the fibers were carefully withdrawn from the buffer solution and were put into a fresh release medium. As expected, more

drug was released from the PCL nanofibers, as shown in Figure 28. In this second assay, about 40% of the retained DOX was released during the first hour in the new medium.

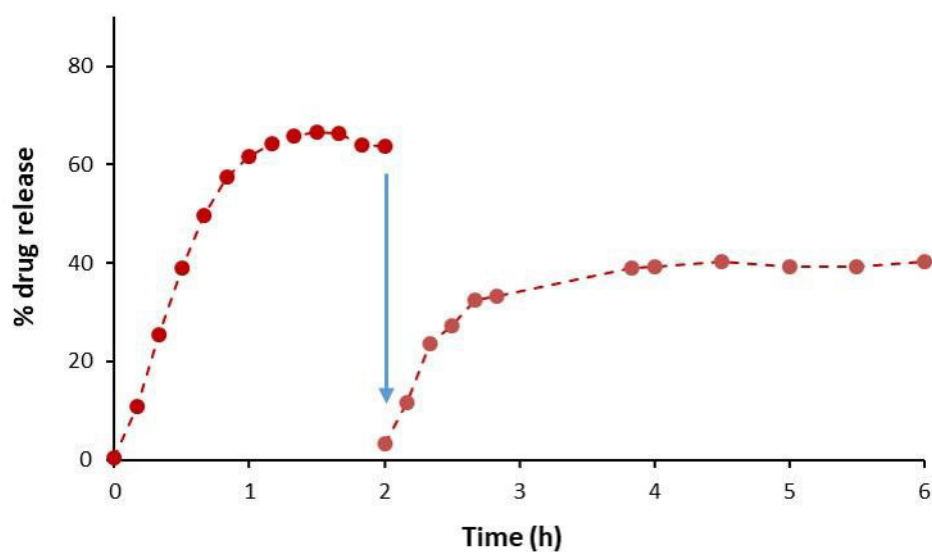


Figure 28– Control release of PCL-DOX (1.75 wt%) nanofibers in buffer pH \approx 5.5. After 2 hours (at the blue arrow point) the fibers were carefully withdrawn from the buffer solution and were put into a fresh release medium. Dashed lines are only eye guides.

Thereby, about 80% of the total amount of DOX encapsulated in the PCL fibers were released at the end of these two assays. It would be possible to continue to place the fibers with the remaining DOX on new release medium and successively obtain an increasing % of DOX released from the nanofibers.

The problem of lack of wettability of the nanofibers would be of great concern if these drug nanocarriers were to be applied in pure aqueous environments. However, the biological medium that will surround the nanofibers in their application sites are cancer cell tissues, with an acidic pH and a membranous/aqueous environment. Therefore, to better mimic this biological environment, the control release assays were also done in micellar medium (sodium lauryl sulfate, SLS 16 mM which is a concentration well above the cmc) with adjusted pH \approx 5.5. Results are shown in Figure 29. In this micro heterogeneous micellar medium the PCL nanofibers become wet very quickly (very small contact angle, impossible to be measured) and the DOX release profile is almost independent of the amount of drug incorporated in the polymeric solution. Again, it is possible to observe a greater % of drug released in the early stages but after it decreases reaching an equilibrium value. In the release conditions used, the partition coefficient, K_p , defined as the ratio between the DOX concentration in the fibers and the DOX concentration in the micellar medium,

reaches values of about 0.6. It should also be noted that the drug release reaches quickly its maximum value, in less than one hour.

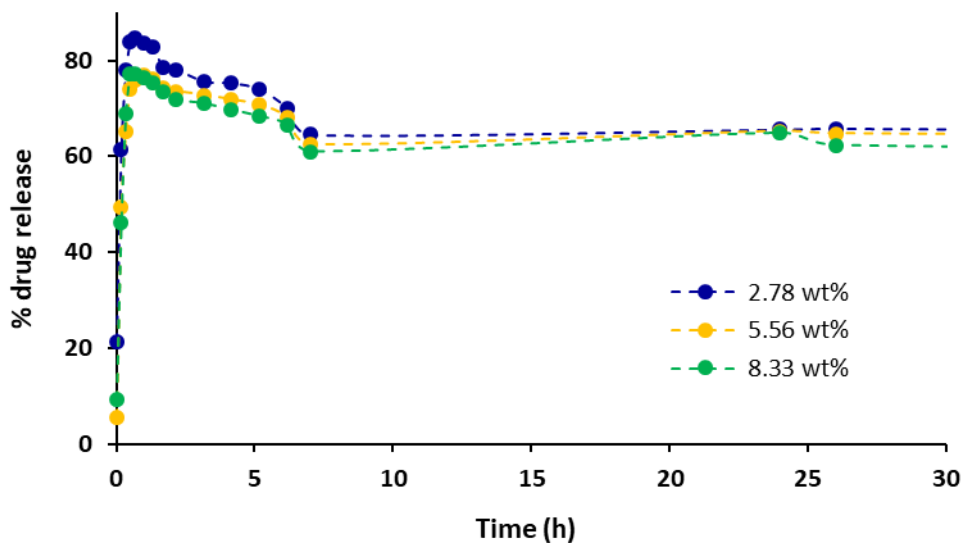


Figure 29– Control release of PCL-DOX nanofibers in micellar medium (SLS 16 mM, pH 5.5) using three different DOX content. Dashed lines are only eye guides.

Having in mind that the therapeutic application of these nanocarriers are in surgical loci or in colorectal cancer, where reduced volumes of physiological fluids are present, another approach for the control release assays was considered. The control release assays were performed confining the nanofiber mats in a dialysis bag. These results are shown in Figure 30 for four different drug contents, using the pH \approx 5.5 buffer as release medium. Results of two replicas are depicted.

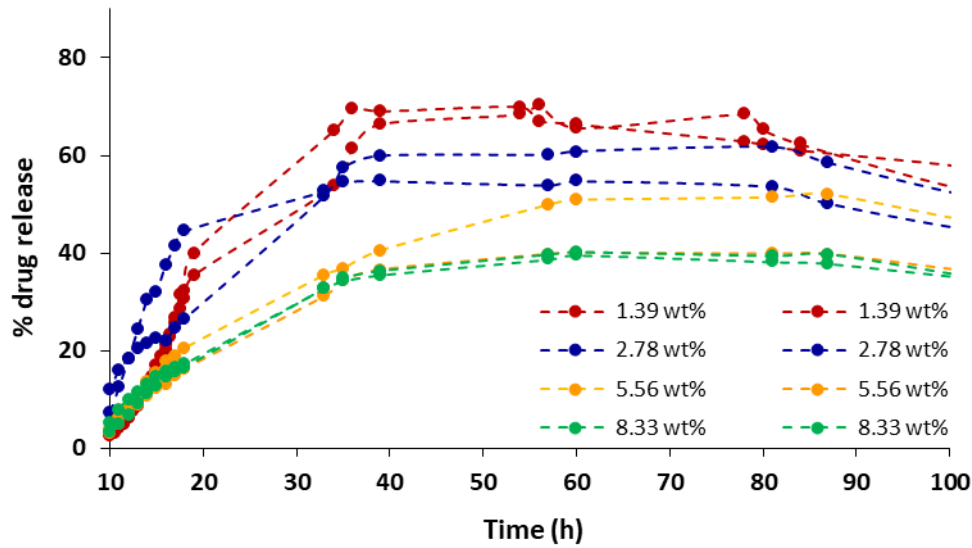


Figure 30– Control release of PCL-DOX nanofibers, confined into a dialysis bag, in buffer pH \approx 5.5, using four different DOX content. Two replicas are depicted for each drug concentration. Dashed lines are only eye guides.

To study the reproducibility of the previous control release assay, six replicas were made for PCL nanofibers containing 1.39 wt% of DOX using the pH \approx 5.5 buffer as release medium. These results are shown in Figure 31. Confining the nanofibers into dialysis bags reduces the variability of the results in comparison to when the nanofibers were put directly into the buffer release medium (compare Figure 31 with Figure 27). The major difference is in the time that the nanofibers take to be wet. Only after 10 hours the nanofibers start to get wet and DOX begins to be released to the medium taking about 30 hours to reach the maximum drug concentration. Again, an equilibrium situation seems to be reached, preventing the complete drug delivery. Once more, it seems that the efficiency of drug release is diminished when the drug content is high, perhaps because nanofibers with higher drug content are more hydrophobic and less wettable.

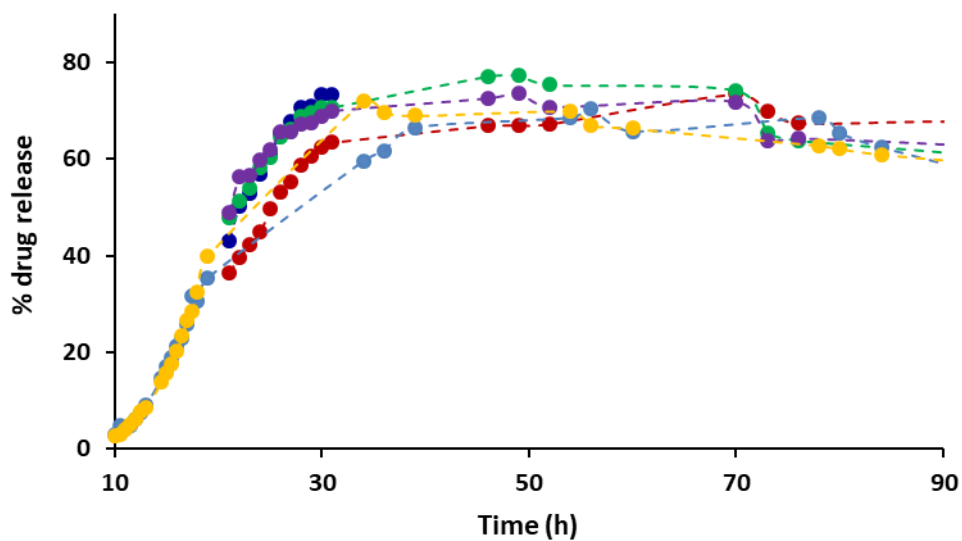


Figure 31 – Control release of PCL-DOX (1.39 wt%) nanofibers, confined into a dialysis bag, in buffer pH \approx 5.5. Six replicas are depicted. Dashed lines are only eye guides.

3.6.4 Cytotoxicity studies of DOX loaded PEO or PCL nanofibers in colorectal cancer cell line

In an attempt to evaluate the therapeutic performance of the developed therapeutic systems, the cytotoxicity of PEO-DOX fibers and PCL-DOX fibers against HCT-116 colorectal tumor cells were assessed *in vitro* by the SRB method. DOX (powder) and nanofibers of PEO and PCL without drug encapsulation were also tested. Results are shown in Figure 32.

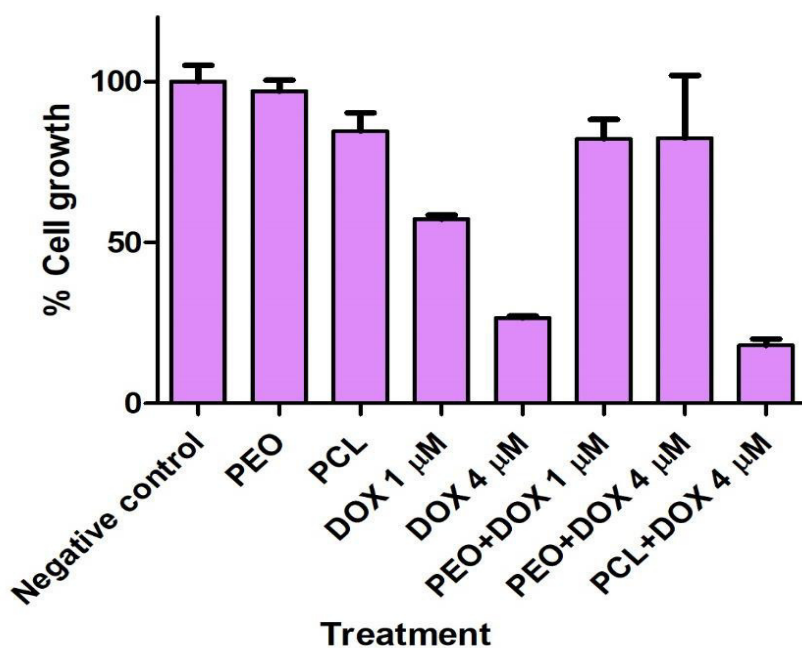


Figure 32 – Cytotoxicity of free DOX and DOX encapsulated into PEO and PCL nanofibers, against HCT-116 colorectal tumour cells.

As can be seen, comparing with the negative control, neat PEO nanofibers are not toxic for the tumor cells and PCL nanofibers are only slightly toxic to these cells. As expected, the cytotoxicity of free DOX increases with the increase of drug concentration and the IC50 is in agreement with the reported values for the same cell line [24]. PCL-DOX nanofibers are very toxic to the HCT cancer cells, as desired and expected, and slightly surpassed the cytotoxicity of the same concentration of the free drug. Contrastingly, PEO-DOX nanofibers have proved to be harmless for the tumor cells under study, at least at the loaded DOX concentrations tested. This is another proof, in addition to the control release results, NMR and ATR-FTIR data, that the complexes formed between PEO and DOX induce drug degradation and consequently cause a loss of drug therapeutic effect.

4 CONCLUSIONS AND FUTURE PERSPECTIVES

Electrospun polymeric nanofibers can be used as nanocarriers for various drugs and bioactive molecules owing to their large surface area and high porosity. Furthermore, the drug release behavior of these materials can be easily controlled by different preparation methods to provide site-specific delivery of drugs.

The encapsulation of DOX, an anticancer drug, in electrospun PEO, PEO-CS and PCL nanofibers was studied. DOX was successfully encapsulated into the nanofibers scaffolds. The nanofibers obtained show a smooth appearance and a random entanglement of the fibers. The average measured diameters were smaller for PEO nanofibers (340 ± 115 nm) than for PCL nanofibers (760 ± 300 nm), and these later nanofibers demonstrated a high porosity, which is already a good indication of a successful drug encapsulation.

A thorough characterization of the nanofibers was performed by several techniques.

XRD, DSC and ATR-FTIR evidenced the presence of DOX in the nanofibers. XRD and DSC analyses demonstrated that the incorporation of DOX into the nanofibers did not affect greatly the crystalline structure of the polymer that suffered a small loss of crystallinity of about 11%. DOX incorporated in the polymeric matrix had also a rigidifying effect, which could be confirmed by the measurement of mechanical properties. These studies also indicated that PCL nanofibers (with or without drug) are much more resilient and elastic than PEO nanofibers. Measurements of the contact angle of a water droplet with the surface of the polymeric scaffold confirmed the distinct water affinity of PEO (hydrophilic) and PCL nanofibers (hydrophobic). DOX incorporation on the nanofibers of PCL increased the contact angle indicating an increase in the surface hydrophobicity.

Despite PEO nanofibers being able to encapsulate DOX, the control release assays have shown that they are inadequate as a controlled release nanosystem for DOX delivery. Indeed, DOX is released almost immediately from PEO, and the combination of this polymer with CS was also not successful since the drug release was almost completely hindered. Furthermore, we found that a strong interaction between PEO and DOX occurs affecting DOX chemical structure, which is essential for DNA intercalation, and for DOX therapeutic effect.

To avoid the problems associated with the degradation of DOX in the presence of PEO, it was encapsulated in PCL nanofibers, and the drug released from this polymeric scaffold was sustained for at least 30 h, as desired. The cytotoxicity assays confirmed the superior therapeutic performance of DOX loaded PCL nanofibers that have shown the strongest cytotoxicity against HCT-116 colorectal tumor cells.

As future prospects, it is envisioned a further optimization of the nanofibers scaffolds, either to include polymeric mixtures that can disrupt under an external stimuli (example when in presence of the acid pH of tumor cells), or to have surface modifications to reduce PCL hydrophobicity and improve its interaction with the cells and biological aqueous media. The great loading capacity of the nanofibers would also allow a future co-encapsulation of another drug or even of a nucleic acid such as siRNA able to provide both chemotherapy and genetic therapy.

Since DOX is widely used in many cancer treatments, it would be also interesting to test the PCL nanosystem in other cancer cell lines to evaluate its therapeutic efficiency in other cancers besides colorectal.

5 BIBLIOGRAPHY

1. Chambers, A.F., A.C. Groom, and I.C. MacDonald (2002). Dissemination and growth of cancer cells in metastatic sites. *Nature Reviews Cancer*, **2**: p. 563-572.
2. Jiang, L., A.M. Nick, and A.K. Sood (2015). Fundamental principles of cancer biology: Does it have relevance to the perioperative period? *Current anesthesiology reports*, **5**(3): p. 250-256.
3. WHO, *GLOBOCAN 2012: Estimated Cancer Incidence, Mortality and Prevalence Worldwide in 2012*, W.H. Organization, Editor. 2012, International Agency for Research on Cancer: Lyon, France.
4. WHO, *Cancer prevention and control in the context of an integrated approach* W.H. Organization, Editor. 2016, WHO.
5. Rowland, J.H., et al. (2013). Cancer survivorship research in Europe and the United States: where have we been, where are we going, and what can we learn from each other? *Cancer*, **119**(0 11): p. 2094-2108.
6. Aggarwal, A., O. Ginsburg, and T. Fojo (2014). Cancer economics, policy and politics: what informs the debate? perspectives from the EU, Canada and US. *Journal of Cancer Policy*, **2**(1): p. 1-11.
7. INE. *Óbitos por algumas causas de morte em Portugal. 2013*. Available from: [https://www.pordata.pt/Portugal/%C3%93bitos+por+algumas+causas+de+morte+\(percentagem\)-758-235710](https://www.pordata.pt/Portugal/%C3%93bitos+por+algumas+causas+de+morte+(percentagem)-758-235710) 2015 accessed on 23-01-2018].
8. Miller, K.D., et al. (2016). Cancer treatment and survivorship statistics, 2016. CA: *A Cancer Journal for Clinicians*, **66**(4): p. 271-289.
9. Haggard, F.A. and R.P. Boushey (2009). Colorectal cancer epidemiology: incidence, mortality, survival, and risk factors. *Clinics in Colon and Rectal Surgery*, **22**(4): p. 191-197.
10. Pinto, C.G., A.T. Paquete, and I. Pissarra (2010). Colorectal cancer in Portugal. *The European Journal of Health Economics*, **10** **Suppl 1**: p. S65-S73.
11. Ponz de Leon, M. and C. Di Gregorio (2001). Pathology of colorectal cancer. *Digestive and Liver Disease*, **33**(4): p. 372-388.
12. Cappell, M.S. (2008). Pathophysiology, clinical presentation, and management of colon cancer. *Gastroenterology Clinics of North America*, **37**(1): p. 1-24.
13. Nikiteas, N.I., et al. (2016). Advances in colorectal cancer. *BioMed Research International*, **2016**: p. 1-2.
14. Hu, T., et al. (2016). Mechanisms of drug resistance in colon cancer and its therapeutic strategies. *World Journal of Gastroenterology*, **22**(30): p. 6876-6889.
15. Yeo, H.L. and P.B. Paty (2014). Management of recurrent rectal cancer: Practical insights in planning and surgical intervention. *Journal of Surgical Oncology*, **109**(1): p. 47-52.
16. Li, S., et al. (2013), MicroRNA-215 inhibits relapse of colorectal cancer patients following radical surgery. *Medical Oncology*, **30**(2): p. 549-554.
17. Sui, X., et al. (2013). Autophagy and chemotherapy resistance: a promising therapeutic target for cancer treatment. *Cell Death & Disease*, **4**(10): p. e838-e850.
18. Enriquez-Navas, P.M., et al. (2016). Exploiting evolutionary principles to prolong tumor control in preclinical models of breast cancer. *Science Translational Medicine*, **8**(327): p. 1-8.
19. Thorn, C.F., et al. (2011). Doxorubicin pathways: pharmacodynamics and adverse effects. *Pharmacogenetics and Genomics*, **21**(7): p. 440-446.
20. Tacar, O., P. Sriamornsak, and C.R. Dass (2013). Doxorubicin: an update on anticancer molecular action, toxicity and novel drug delivery systems. *Journal of Pharmacy and Pharmacology*, **65**(2): p. 157-170.

21. Khaleel, S.A., et al. (2016). Didox and resveratrol sensitize colorectal cancer cells to doxorubicin via activating apoptosis and ameliorating P-glycoprotein activity. *Scientific Reports*, **6**: p. 36855-36866.
22. Zhang, M., et al. (2016). Edible ginger-derived nano-lipids loaded with doxorubicin as a novel drug-delivery approach for colon cancer therapy. *Molecular Therapy*, **24**(10): p. 1783-1796.
23. Weinlander, G., et al. (1997). Treatment of advanced colorectal cancer with doxorubicin combined with two potential multidrug-resistance-reversing agents: high-dose oral tamoxifen and dexverapamil. *Journal of Cancer Research and Clinical Oncology*, **123**(8): p. 452-455.
24. Lüpertz, R., et al. (2010). Dose- and time-dependent effects of doxorubicin on cytotoxicity, cell cycle and apoptotic cell death in human colon cancer cells. *Toxicology*, **271**(3): p. 115-121.
25. Li, W., et al. (2014). Targeted delivery of doxorubicin using a colorectal cancer-specific ssDNA aptamer. *The Anatomical Record*, **297**(12): p. 2280-2288.
26. Speth, P.A.J., Q.G.C.M. van Hoesel, and C. Haanen (1988). Clinical pharmacokinetics of doxorubicin. *Clinical Pharmacokinetics*, **15**(1): p. 15-31.
27. Zhu, H., et al. (2016). Doxorubicin redox biology: redox cycling, topoisomerase inhibition, and oxidative stress. *Reactive Oxygen Species*, **1**(3): p. 189-198.
28. Yang, F., et al. (2014). Doxorubicin, DNA torsion, and chromatin dynamics. *Biochimica et biophysica acta*, **1845**(1): p. 84-89.
29. Chen, N.-T., et al. (2012). Probing the dynamics of doxorubicin-DNA intercalation during the initial activation of apoptosis by Fluorescence Lifetime Imaging Microscopy (FLIM). *PLOS ONE*, **7**(9): p. e44947-e44955.
30. Airoldi, M., et al. (2014). Interaction of doxorubicin with polynucleotides. A spectroscopic study. *Biochemistry*, **53**(13): p. 2197-2207.
31. Barenholz, Y., et al. (1993). Stability of liposomal doxorubicin formulations: Problems and prospects. *Medicinal Research Reviews*, **13**(4): p. 449-491.
32. Barenholz, Y. (2007). Amphipathic weak base loading into preformed liposomes having a transmembrane ammonium ion gradient: from the bench to approved Doxil, in *Liposome technology: entrapment of drugs and other materials into liposomes*, G. Gregoriadis, Editor, Taylor & Francis: University of Michigan. p. 1-25.
33. Tiwari, G., et al. (2012). Drug delivery systems: An updated review. *International Journal of Pharmaceutical Investigation*, **2**(1): p. 2-11.
34. Davis, M.E., Z. Chen, and D.M. Shin (2008). Nanoparticle therapeutics: an emerging treatment modality for cancer. *Nature Reviews Drug Discovery*, **7**: p. 771-782.
35. Pérez-Herrero, E. and A. Fernández-Medarde (2015). Advanced targeted therapies in cancer: drug nanocarriers, the future of chemotherapy. *European Journal of Pharmaceutics and Biopharmaceutics*, **93**: p. 52-79.
36. Chen, Z., et al. (2016). Electrospun nanofibers for cancer diagnosis and therapy. *Biomaterials Science*, **4**(6): p. 922-932.
37. Xu, X., et al. (2008). The release behavior of doxorubicin hydrochloride from medicated fibers prepared by emulsion-electrospinning. *European Journal of Pharmaceutics and Biopharmaceutics*, **70**(1): p. 165-170.
38. Liu, S., et al. (2013). Inhibition of orthotopic secondary hepatic carcinoma in mice by doxorubicin-loaded electrospun polylactide nanofibers. *Journal of Materials Chemistry B*, **1**(1): p. 101-109.
39. Qiu, K., et al. (2013). Doxorubicin-loaded electrospun poly(l-lactic acid)/mesoporous silica nanoparticles composite nanofibers for potential postsurgical cancer treatment. *Journal of Materials Chemistry B*, **1**(36): p. 4601-4611.

40. Yohe, S.T., et al. (2012). 3D Superhydrophobic electrospun meshes as reinforcement materials for sustained local drug delivery against colorectal cancer cells. *Journal of controlled release*, **162**(1): p. 92-101.
41. Bakhtiari, M., et al. (2017). Development of novel doxorubicin loaded biodegradable polymeric nanofibers as the anticancer drug delivery systems. *BioNanoScience*, : p. 1-7.
42. Zamani, M., M.P. Prabhakaran, and S. Ramakrishna (2013). Advances in drug delivery via electrospun and electrosprayed nanomaterials. *International Journal of Nanomedicine*, **8**: p. 2997-3017.
43. Xu, X., et al. (2009). Ultrafine PEG–PLA fibers loaded with both paclitaxel and doxorubicin hydrochloride and their in vitro cytotoxicity. *European Journal of Pharmaceutics and Biopharmaceutics*, **72**(1): p. 18-25.
44. Sill, T.J. and H.A. von Recum (2008). Electrospinning: Applications in drug delivery and tissue engineering. *Biomaterials*, **29**(13): p. 1989-2006.
45. Ardeshirzadeh, B., et al. (2015). Controlled release of doxorubicin from electrospun PEO/chitosan/graphene oxide nanocomposite nanofibrous scaffolds. *Materials Science and Engineering: C*, **48**: p. 384-390.
46. Zheng, F., et al. (2013). Antitumor efficacy of doxorubicin-loaded electrospun nano-hydroxyapatite-poly(lactic-co-glycolic acid) composite nanofibers. *Polymer Chemistry*, **4**(4): p. 933-941.
47. Zhang, J., et al. (2016). Antitumor activity of electrospun polylactide nanofibers loaded with 5-fluorouracil and oxaliplatin against colorectal cancer. *Drug Delivery*, **23**(3): p. 784-790.
48. Yuan, Z., et al. (2016). Doxorubicin-loaded mesoporous silica nanoparticle composite nanofibers for long-term adjustments of tumor apoptosis. *Nanotechnology*, **27**(24): p. 245101-245111.
49. Yu, Y., et al. (2015). Antitumor Activity of Doxorubicin-Loaded Carbon Nanotubes Incorporated Poly(Lactic-Co-Glycolic Acid) Electrospun Composite Nanofibers. *Nanoscale Research Letters*, **10**(1): p. 343.
50. Zeng, J., et al. (2005). Influence of the drug compatibility with polymer solution on the release kinetics of electrospun fiber formulation. *Journal of Controlled Release*, **105**(1): p. 43-51.
51. Lu, T., et al. (2011). Doxorubicin-loaded ultrafine PEG-PLA fiber mats against hepatocarcinoma. *Journal of Applied Polymer Science*, **123**(1): p. 209-217.
52. Doustgani, A. (2017). Doxorubicin release from optimized electrospun polylactic acid nanofibers. *Journal of Industrial Textiles*, **47**(1): p. 71-88.
53. Yan, E., et al. (2014). Biocompatible core–shell electrospun nanofibers as potential application for chemotherapy against ovary cancer. *Materials Science and Engineering: C*, **41**: p. 217-223.
54. Kim, Y.-J., M. Ebara, and T. Aoyagi (2013). A smart hyperthermia nanofiber with switchable drug release for inducing cancer apoptosis. *Advanced Functional Materials*, **23**(46): p. 5753-5761.
55. Salehi, R., et al. (2013). Stimuli-responsive nanofibers prepared from poly(N-isopropylacrylamide-acrylamide-vinylpyrrolidone) by electrospinning as an anticancer drug delivery. *Designed Monomers and Polymers*, **16**(6): p. 515-527.
56. Fuertges, F. and A. Abuchowski (1990). The clinical efficacy of poly(ethylene glycol)-modified proteins. *Journal of Controlled Release*, **11**(1): p. 139-148.
57. Working, P.K., et al. (1997), Safety of Poly(ethylene glycol) and Poly(ethylene glycol) Derivatives, in Poly(ethylene glycol) in *American Chemical Society*. p. 45-57.
58. Kim, J., et al. (2006). Synthesis of PEO-Based Materials for Biomedical Applications. *Macromolecular Symposia*, **245-246**(1): p. 565-570.
59. Wang, X., et al. (2013). Crystalline Morphology of Electrospun Poly(ε-caprolactone) (PCL) Nanofibers. *Industrial & Engineering Chemistry Research*, **52**(13): p. 4939-4949.

60. Barenholz, Y. (2012). Doxil® — The first FDA-approved nano-drug: Lessons learned. *Journal of Controlled Release*, **160**(2): p. 117-134.
61. Huang, Z.-M., et al. (2003). A review on polymer nanofibers by electrospinning and their applications in nanocomposites. *Composites Science and Technology*, **63**(15): p. 2223-2253.
62. Lima, R.B. (2013), Nanofibras de Materiais Biológicos. Dissertação de mestrado, *Escola de Engenharia*. Universidade do Minho: Braga, Portugal.
63. Karbasi, S., et al. (2016). Evaluation of structural and mechanical properties of electrospun nano-micro hybrid of poly hydroxybutyrate-chitosan/silk scaffold for cartilage tissue engineering. *Advanced Biomedical Research*, **5**: p. 180-196.
64. Sreedhara, S.S. and N.R. Tata (2013). A novel method for measurement of porosity in nanofiber mat using pycnometer in filtration. *Journal of Engineered Fibers and Fabrics*, **8**(4): p. 132-137.
65. Yang, A., R. Wu, and P. Zhu (2001). Thermal analysis and miscibility of chitin/polycaprolactone blends. *Journal of Applied Polymer Science*, **81**(13): p. 3117-3123.
66. Lai, W.-C. and W.-B. Liau (2004). Study of the miscibility and crystallization behavior of poly(ethylene oxide)/poly(vinyl alcohol) blends. *Journal of Applied Polymer Science*, **92**(3): p. 1562-1568.
67. Sánchez-Soto, P.J., et al. (2002). Effect of molecular mass on the melting temperature, enthalpy and entropy of hydroxy-terminated PEO. *Journal of Thermal Analysis and Calorimetry*, **67**(1): p. 189-197.
68. Kunjachan, S., et al. (2011). Chitosan-based macrophage-mediated drug targeting for the treatment of experimental visceral leishmaniasis. *Journal of Microencapsulation*, **28**(4): p. 301-310.
69. Borjigin, M., et al. (2013). Electrospun fiber membranes enable proliferation of genetically modified cells. *International Journal of Nanomedicine*, **8**: p. 855-864.
70. Elzein, T., et al. (2004). FTIR study of polycaprolactone chain organization at interfaces. *Journal of Colloid and Interface Science*, **273**(2): p. 381-387.
71. Das, G., et al. (2010). FT-IR, Raman, RRS measurements and DFT calculation for doxorubicin. *Microscopy Research and Technique*, **73**(10): p. 991-995.
72. Adam, N.K. (1957). Use of the term 'Young's equation' for contact angles. *Nature*, **180**: p. 809-810.
73. Nuraje, N., et al. (2013). Superhydrophobic electrospun nanofibers. *Journal of Materials Chemistry A*, **1**(6): p. 1929-1946.
74. Huang, F., et al. (2008). Surface structures and contact angles of electrospun poly(vinylidene fluoride) nanofiber membranes. *International Journal of Polymer Analysis and Characterization*, **13**(4): p. 292-301.
75. Chen, G., et al. (2015). Core-shell structure PEO/CS nanofibers based on electric field induced phase separation via electrospinning and its application. *Journal of Polymer Science Part A: Polymer Chemistry*, **53**(19): p. 2298-2311.
76. Sun, K. and Z.H. Li (2011). Preparations, properties and applications of chitosan based nanofibers fabricated by electrospinning. *Express Polymer Letters*, **5**: p. 342-361.
77. Gupta, P.K., F.C. Lam, and C.T. Hung (1988). Investigation of the stability of doxorubicin hydrochloride using factorial design. *Drug Development and Industrial Pharmacy*, **14**(12): p. 1657-1671.
78. Kaushik, D. and G. Bansal (2015). Four new degradation products of doxorubicin: an application of forced degradation study and hyphenated chromatographic techniques. *Journal of Pharmaceutical Analysis*, **5**(5): p. 285-295.
79. Zutshi, A. (1994) Physicochemical characterization and stability of doxorubicin in aqueous solutions, University of Florida. p. 440.

80. Tomlinson, E. and L. Malspeis (1982). Concomitant adsorption and stability of some anthracycline antibiotics. *Journal of Pharmaceutical Sciences*, **71**(10): p. 1121-1125.
81. Wood, M.J., W.J. Irwin, and D.K. Scott (1990). Stability of doxorubicin, daunorubicin and epirubicin in plastic syringes and minibags. *Journal of Clinical Pharmacy and Therapeutics*, **15**(4): p. 279-289.
82. Wu, D.C. and C.M. Ofner (2013). 3rd, Adsorption and degradation of doxorubicin from aqueous solution in polypropylene containers. *AAPS PharmSciTech*, **14**(1): p. 74-77.
83. Ducheyne, P., et al. (2015). *Comprehensive Biomaterials*. Elsevier Science.
84. Xiang, F., et al., *Structural tailoring of hydrogen-bonded poly(acrylic acid)/poly(ethylene oxide) multilayer thin films for reduced gas permeability*. *Soft Matter*, 2015. **11**(5): p. 1001-1007.
85. Azevedo, H.S. and R.L. Reis (2005). Understanding the enzymatic degradation of biodegradable polymers and strategies to control their degradation rate, in *Biodegradable Systems. Tissue Engineering and Regenerative Medicine*. p. 177-201.
86. Martins, A.M., et al. (2009). The role of lipase and α -amylase in the degradation of starch/poly(ϵ -caprolactone) fiber meshes and the osteogenic differentiation of cultured marrow stromal cells. *Tissue Engineering. Part A*, **15**(2): p. 295-305.
87. Tokiwa, Y., et al. (2009). Biodegradability of plastics. *International Journal of Molecular Sciences*, **10**(9): p. 3722-3742.